https://doi.org/10.5194/gmd-2022-292
Preprint. Discussion started: 16 December 2022

Geoscientific Model Development Discussions

Can TROPOMI-NO_2 satellite data be used to track the drop and resurgence of NO_x emissions between 2019 - 2021 using the multi-source plume method (MSPM)?

Enrico Dammers[1], Janot Tokaya[1], Christian Mielke[2], Kevin Hausmann[2], Debora Griffin[3], Chris McLinden[3], Henk Eskes[4], and Renske Timmermans[1]

[1]Netherlands Organisation for Applied Scientific Research (TNO), Utrecht, Princetonlaan 6, 3584 CB, The Netherlands
[2]Umweltbundesamt (UBA), Dessau-Roßlau, Wörlitzer Pl. 1, 06844, Germany
[3]Air Quality Research Division, Environment and Climate Change Canada, 4905 Dufferin St, M3H 5T4, Toronto, Canada
[4]KNMI, De Bilt, Utrechtseweg 297, 3731 GA, The Netherlands

Correspondence: Enrico Dammers (enrico.dammers@tno.nl)

Abstract. NO_x is an important primary air pollutant, dominantly produced by anthropogenic, mostly combustion based, activities from sectors such as industry, traffic and transport. NO_x is directly linked to negative health and environmental impacts. Currently, the construction of emission inventories to keep track of NO_x emissions is based on official national reported emissions and proxies such as activity data as well as direct measurements. The effort to properly construct an accurate inventory is significant and time consuming which causes a reporting offset between one and five years with respect to the current date. Next to this temporal lag difficulties in composed inventories can arise from legislative and protocol differences between countries and over time in reporting of emissions. Satellite based atmospheric composition measurements provide a unique opportunity to fill this gap and independently estimate emissions on a large scale in a consistent, transparent and comprehensible way. They give the possibility to check for compliance with emission reduction targets in a timely manner as well as to observe rapid emission reductions such as experienced during the COVID-19 lock-downs. In this study we apply a consistent methodology to derive NO_x emissions over Germany for the years of 2019-2021. For the years where reporting is available differences between satellite estimates and inventory totals were within 100kt. The large reduction of NO_x emissions related to the COVID-19 lock-downs were observed in both the inventory and satellite derived emissions. The recent projections for the inventory emissions pointed to a recovery of the emissions towards pre-COVID19 levels this increase was not observed. While emissions from the larger power-plants did rebound to earlier levels, others sectors such as road transport and shipping did not and could be linked to a reduction in the number of heavier transport trucks. This again illustrates the value of having a consistent satellite based methodology for faster projections to guide and check the conventional emission inventory reporting. The method described in this manuscript also meet the demand for independent verification of the official emission inventories, which will enable inventory compilers to detect potentially problematic reporting issues. Transparency and comparability, two key values for emission reporting, are thus bolstered by this technique.

https://doi.org/10.5194/gmd-2022-292
Preprint. Discussion started: 16 December 2022

Geoscientific Model Development Discussions

1 Introduction

Nitrogen monoxide (NO) and dioxide (NO_2) play an important role in atmospheric chemistry as they influence the abundance of tropospheric ozone (Crutzen et al., 1970) and lead to aerosol formation. These primary air pollutants are collectively called nitrogen oxides ($NO_x \equiv NO + NO_2$). Since NO_2 is formed primarily through rapid oxidation of NO their concentrations are strongly related. NO_2 is a major source of air pollution and exposure to high concentrations can result in nausea, dyspnoea, headache and respiratory disease that cause an association between long-term exposure and reduced live expectancy (Atkinson et al., 2018; Belch et al., 2021). Hence objective limits are set by the European union on the hourly (200 $\mu g m^{-3}$) and yearly (40 μg m^{-3}) NO_2 exposure levels with recent WHO limits reducing this level further to 10 μg m^{-3}(yearly,Organization et al. (2021)). Next to these adverse health effect NO_2 causes a strain on the environment through soil and water acidification as well as eutrophication.

Many anthropogenic activities contribute to the atmospheric NO_2 concentration because NO_2 is formed in combustion processes where air (being about 80% nitrogen) is the oxidant. Natural sources of NO_x include lightning and soil emissions. The main sources of NO_2 emissions are the internal combustion engines that burn fossil fuels in motor vehicles and industry. The overall atmospheric evolution and budget of NO_x in the atmosphere has been determined with ever-increasing accuracy over the last decades. National environmental agencies are required to monitor the level of NO_x and the contribution of human activity on it according to international agreements, such as the Geneva Convention on Long-Range Transboundary Air Pollution (Nations., 1979.). Efforts undertaken to limit NO_x emissions have resulted in strong reductions of ambient NO_2 concentration in many parts of the world (Jamali et al., 2020).

Inventories of NO_x emissions are commonly compiled using a bottom-up approach based on proxies as well as direct emission measurements, for example in stacks. Retrieving data at detailed levels as well as creation of representative emission factors that translate an activity into emissions is, however, a very labour intensive task. Emissions from road transport for example depend on several factors such as: fleet composition, type of fuel, engine maintenance and design, outside temperature, usage profile and road conditions. New technology standards, reported numbers, and real life measures (or lack thereof compared to projections) are slow to be incorporated in the emission inventories, as they need to fulfill the good practice guidelines of the respective protocol commonly agreed upon by the member states. Therefore, inventories cannot reflect the latest actual emission trends in "near-real-time". This is problematic especially when large deviations from business as usual scenarios occur, which are then only reflected in the inventories with a great time lag. For example air quality applications such as forecasts depend on accurate emission inventories to represent these changes. A recent example is the large changes in emissions following the 2020 COVID lock-downs and the post lockdown recovery phase of the emissions, which both are poorly represented in current air quality applications (Goldberg et al., 2020; Griffin et al., 2020; Barré et al., 2021).

A potential solution to speed up the creation of up to date emissions from inventories, in a harmonized way, is the usage of satellite observations of air pollutants (Beirle et al., 2011; Fioletov et al., 2011; Mijling et al., 2009; Miyazaki et al., 2012; McLinden et al., 2016; Goldberg et al., 2019; Griffin et al., 2020; Dammers et al., 2019; Ding et al., 2020) which can be used to verify the reported emissions, constrain emission sources, and analyse trends. Over the past decade the data availability of

https://doi.org/10.5194/gmd-2022-292
Preprint. Discussion started: 16 December 2022


Geoscientific Model Development Discussions

satellite-based atmospheric composition measurements has increased tremendously. Furthermore, due to an increase in instrument sensitivity, spatial and temporal resolution these satellite-based measurements are becoming more and more attractive for air quality monitoring and emission studies. Recent scientific developments have shown the viability of various methods in estimating emissions based on satellite observations. In the case of NO_x, the earliest methods were mostly aimed to individual point sources (Beirle et al., 2011) followed by regional estimates at lower spatial resolutions (Mijling et al., 2009; Miyazaki et al., 2012). The more recent TROPOspheric Monitoring Instrument (TROPOMI) with its unprecedented horizontal resolution improved the resolvability of individual and clusters of emission sources (Ding et al., 2020; McLinden et al., 2022).

Here, we apply one of the more recently developed methods (Fioletov et al., 2017) to TROPOMI-NO_2 observations to derive the NO_x emissions for Germany for the period of 2019-2021. The plume based fitting method relies on wind data and a parameterization of multiple Gaussian plumes originating from corresponding point sources to estimate the strength of the emissions at these point source location. These estimates are then compared to the emissions in the current inventories for 2019 and 2020 as well as the projected emissions (latest draft) of 2021 to assess their validity and analyse the expected variations due to the COVID lock-downs. The plume based fitting routine is part of an open-access standalone offline tool. Besides the plume based fitting routine two further methods were implemented during the development phase, a simple mass-balance approach, for which we coined the term "naive method", and the divergence approach as described by (Beirle et al., 2016). Furthermore, the simple mass-balanced method was employed into an online web-tool (space-emissions, described further in the manuscript), geared towards emission inventory agencies that are interested to compare their national total emissions to an independent, yet easily comprehensible space-borne measurement. More details on the implementation and comparison of these (other) methods can be found in (Dammers et al., 2022b). In this study we focus on the plume based fitting method.

2 Methodology and Datasets

A major aim behind the research work presented here was the provision of a tool, developed for the Umweltbundesamt (UBA), to compare satellite-derived emissions to inventory emissions for air pollutants to verify the bottom-up computed emissions with independent data from space-borne measurements.This should help inventory compilers to build trust in their work and identify potentially problematic issues, should there be large deviations between inventory data and space-borne data trends. Furthermore, the tool should allow for fast checks if a country is compliant with its national air pollutant reduction targets, which have been initiated by EU decisions e.g.: (EU, 2022) or if adjustments need to be made as exemplified and discussed in (Dore, 2022). The national inventory data is reported through the informative inventory report (IIR): For the case of Germany it is publicly available from its original source:
https://iir.umweltbundesamt.de/2022/. The TROPOMI-NO_2 product offers an inventory independent source to verify NO_x emissions. These space-borne observations of spatio-temporal trends offer the possibility for inventory agencies to independently check their findings on e.g. emission reduction of NO_x throughout the country without having to rely on bottom-up inventory data products, such as the Emission Database for Global Atmospheric Research (EDGAR) (Crippa et al., 2019), the Copernicus Atmospheric Monitoring Service (CAMS) database (Granier et al., 2019; Kuenen et al., 2022), or other country

https://doi.org/10.5194/gmd-2022-292
Preprint. Discussion started: 16 December 2022


Geoscientific Model Development Discussions

specific gridded data products e.g. from the Gridding Emission Tool for ArcGis (GRETA) (Schneider et al., 2016). Fast changing spatio-temporal patterns may only be captured by space-borne data in a timely manner in comparison to the above named gridded data products.

2.1 Data sets

2.1.1 Emission inventory

The reporting of the national air pollutants follows international guidelines that are available via the EMEP centre on Emission Inventories and Projections (https://www.ceip.at/reporting-instructions). The reported inventory data for Germany, in form of the detailed informative inventory report (IIR), detailing the technical methodology, may be found here: https://iir.umweltbundesamt.de/2022/. The data is arranged in time series per gas species considering the different emission sources of NO_x in sectors such as e.g. public power, industry and traffic in very detailed, dis-aggregated form, at the national level. The bottom up creation of these data is driven by statistical data, provided by e.g. the German statistical authority (DESTASIS) and complex models that use this data to compile the emissions for a specific gas (or aerosol) for a specific emission source in a specific sector and year. The uncertainties for each reported emission source depend on the availability of the data used for the emission calculation, and may vary considerably. As an example, uncertainties in emissions from sectors, which are quite accurately described by statistical data and models, such as emissions from large power plants, show much lower uncertainties than sectors that are governed by a great complexity such as the natural variability of NO_x from agricultural emissions in soils (e.g.uncertainties can be more than 300 percent for Agricultural Soils). Though TROPOMI emission estimates provided by this project may not be suitable to resolve these issues of specific sectors they may, however, contribute to identify problems with reported emission totals e.g. should the temporal trend between the inventory data and TROPOMI data diverge significantly. Otherwise the tool is able to build confidence and trust into the emission inventory, should both trends (the TROPOMI based emission estimates and the national total) match. In this study both the gridded (CLRTAP, 2021) and non-gridded inventory (CLRTAP, 2022) reported emission data sets are used, retrieved directly from the respective Convention on Long-range Transboundary Air Pollution (CLRTAP) inventories which follow the nomenclature for reporting (NFR) standard. The gridded data set is only available for 2019 while the non-gridded data is available for both 2019 and 2020. The 2021 data is a prognosis based on the trends observed between 2012-2019 for all emission classes, under the assumption that the patterns in most emission sectors rebound after the 2020 COVID lock-downs. An overview of relative contributions of individual sectors to the total gridded emissions is shown by sector in Fig. A1.

All emissions except the MEMO items (additional reported emissions on non-standard emission such as volcanoes, forest fires etc) are selected from the CLRTAP inventories. To this set two natural sources are added, namely non-agricultural soils and lightning. Globally the lightning NO constitutes about 3% of the total NO_x emission budget. Please note that according to the guidebook (EEA, 2019) only 20% of the lightning NO is formed in the lowest 1000 meter of the atmosphere and the remaining 80% at higher altitude (all inter cloud lightning above 5 km height) (EEA, 2019). A rough estimate for the lightning emissions can be made on the basis of the number of flashes per km^2 and the expected mol NO_x released per flash. A study by Anderson

https://doi.org/10.5194/gmd-2022-292
Preprint. Discussion started: 16 December 2022


Geoscientific Model Development Discussions

and Klugmann (2014) gives an average of about 2 flashes per km^2 throughout Germany, with fewer flashes in the central and northern parts. Assuming that on average the number of lightning flashes did not increase significantly in combination with a production of about 180 mol NO_x/flash (Bucsela et al., 2019) and German surface area of about 357.000 km^2, gives us a German lightning NO_x emission total of about 5 kt NO_x per year. This emission total is very minor and spread out over a large domain, and not expected to be a significant source of error when comparing the satellite derived emission estimates with the emission inventory.

Due to widespread nitrogen pollution and deposition in Germany it is complicated to make an estimate of purely non-anthropogenic and non-agricultural soil emissions. There are several studies that looked at soil NO_x emissions for the European domain, mostly based on the anthropogenic emissions Yienger and Levy II (1995), but fewer that focus on purely natural emissions. Simpson et al. (1999) gave an estimate of 3-90 kt NO_x of forest emissions and 20 kt NO_x for grassland soils. This estimate was more recently updated by Simpson and Darras (2021) and is available as the CAMS-GLOB-SOIL inventory (Simpson, 2022), with a reported 2018 German emission total of about 160 kt NO_x. Within the inventory the emissions are split between fertilizer induced, biome, deposition related, and pulsed soil emissions. There is always a danger of double counting such emissions but the fertilizer induced emissions of 100 kt match closely to those included within the 2019 GNFR data of about 110 kt (classed under L. AgriOther sources). The remaining 60kt of NO_x per year is a combination of biome, deposition related, and pulsed soil emissions. The distribution of non-agricultural source emissions are quite uniformly distributed throughout Germany, peaking somewhat towards the northeastern part of the country. Note that Simpson and Darras (2021) stress that the derived soil emissions still have a large uncertainty range, mostly related to a lack of observations, missing data for some biomes, and the uncertainty of input parameters such as soil temperatures. Annual variations are expected to be large depending on variations in soil temperatures. Simpson and Darras (2021) do not provide an upper and lower range of the emissions.

Additionally, we use the European Pollutant Release and Transfer Register (E-PRTR) for the locations and emission strength of the largest industrial emission sources within Germany. The latest data set (v18) can be accessed via: https://www.eea.europa.eu/data-and-maps/data/industrial-reporting-under-the-industrial-6. Only sources with an emission strength above 0.25 kt NO_x per year are selected for later comparison to the satellite derived emissions. Note, that the most recent data available is based on reported emissions of the year 2017, and thus we only use the data as a rough indication of source strength.

2.1.2 TROPOMI-NO_2

The TROPOMI instrument, on board of the S5P satellite platform, was launched on the 13th of October 2017. The satellite instrument achieves almost full daily coverage of the globe through a sun-synchronous orbit with a local overpass at around 13:30 (Veefkind et al., 2012). TROPOMI has an unprecedented horizontal resolution of $3.5 \times 5.5\,km^2$ for the NO_2 product. Details on the retrieval are described in the Copernicus user manuals (ATBD) as well as in earlier publications such as van Geffen et al. (2022). The TROPOMI-NO_2 standard product has several data streams, with the near-real-time product available within 3 hours (NRTI), the offline(OFFL) (2019-2021) reprocessed version following one day later. A complete reprocessed version is provided at more irregular intervals (RPRO, April 2018-November 2018). Finally, a reanalysis of the full data set

https://doi.org/10.5194/gmd-2022-292
Preprint. Discussion started: 16 December 2022

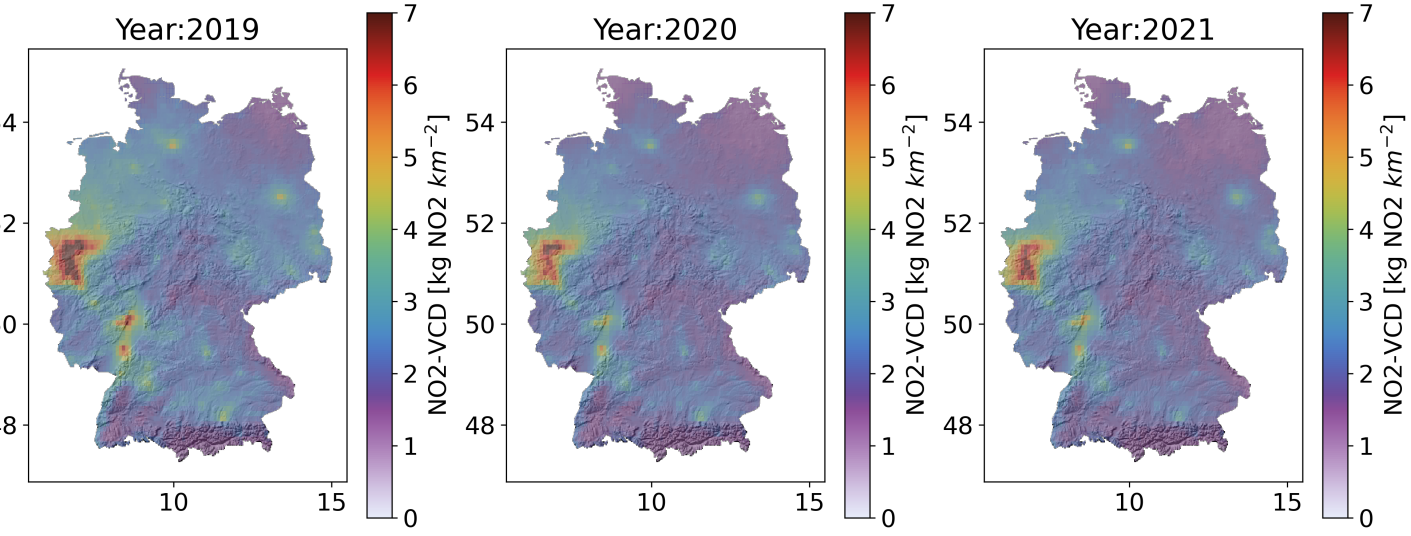

Figure 1. TROPOMI-NO_2 (PAL, v2.3.1) yearly averages for 2019-2021.

became available at the end of 2021, named the PAL product, which is currently available until the end of November 2021, connecting seamlessly to OFFL v2.3.1 from November 2021 to July 2022. The TROPOMI-NO_2 product went through several upgrades concerning its product versions over the years, with the most recent three upgrades from version v1.3.2 to version v1.4.0, then v2.2.0, then v2.3.1, and v2.4.0 taking place in November 2020, July 2021, November 2021 and July 2022. The most recent upgrade to version 2 involved a more major overhaul greatly improving the overall quality of the retrieval (van Geffen et al., 2022; Zhao et al., 2022). The TROPOMI-NO_2-PAL product includes a reanalysis of the earlier data and provides a consistent version throughout (v2.3.1). This product is recommended to be used for any longer time series analysis and has been used in this study. We combine this product with 2 months of the newest OFFL data (v2.3.1) to complete the data series for 2021. The PAL product is available through the PAL data portal (https://data-portal.s5p-pal.com/products/no2.html). The quality of the TROPOMI-NO_2 PAL and OFFL products based on the v2.3.1 processor version is discussed by (van Geffen et al., 2022). Furthermore, the previous data set versions 1.2.x and 1.3.x were relatively well validated (Verhoelst et al., 2021). The TROPOMI NO_2 data are typically well correlated but show an underestimation of the tropospheric column when compared to ground-based MAX-DOAS and PANDORA instruments (Verhoelst et al., 2021). The median negative bias ranges from -15 to -35% in most clean to slightly polluted regions up to -50% over highly polluted regions for versions 1.2.x and 1.3.x. This bias is reduced in the PAL data set (van Geffen et al., 2022) with reported improvements for the tropospheric columns from an average low bias of -32% to -23%. The range of the differences for individual sites are however quite wide with for example the MAX-DOAS in de Bilt, the Netherlands, showing a range of around -75 up to around +50% (25 and 75% percentiles) with a median of around -20%. The negative bias can be explained by the low spatial resolution of the a-priori profiles as well as the treatment of clouds and aerosols in the retrieval. As for the TROPOMI data quality criteria, the recommended set were used, which means only observations with a cloud fraction below 0.3 were used, based on

https://doi.org/10.5194/gmd-2022-292
Preprint. Discussion started: 16 December 2022


Geoscientific Model Development Discussions

the cloud_fraction_crb_nitrogendioxide_window variable in the data files. Furthermore, observations with a quality value (qa_value) below 0.75 were filtered from the data set.

Figure 1 shows yearly averages of the TROPOMI-NO2 (PAL, v2.3.1) data. Here the impact of the COVID-19 lockdown measures in 2020 is clearly visible: The industrialized Ruhr valley at the western border of Germany shows far reduced levels of NO_2, if compared to 2019. The same is also observed in the industrial centers further to the South-South-West, which almost vanishes in 2020 and show only a very slow recovery of emissions in 2021.

2.1.3 Meteorology

The methodology in this study makes use of the wind rotation approach as explained in detail in Pommier et al. (2013), Fioletov et al. (2015), and Dammers et al. (2019). The required meteorology is taken from ECMWF's ERA-5 dataset (https://cds.climate.copernicus.eu/cdsapp#!/dataset/reanalysis-era5-pressure-levels?tab=overview (Hersbach et al., 2020, 2018)) which was downloaded at a resolution of 0.25ºx0.25º resolution and 1-hour temporal resolution. To match each of the satellite footprints the meteorological fields are interpolated (spatially and temporally) to each of the observations. We assume that the majority of the NO_x mass from local emissions is located in the lower boundary layer (Beirle et al., 2016; McLinden et al., 2022; Griffin et al., 2020) and for the transport of NO_x an average is taken of the wind fields of the first 100 hPa (around the first kilometre) above the surface. These are approximately the levels between ∼1000-900 hPa for a typical sea level location, and for a location with a surface pressure of 800 hPa, winds between 800 and 700 hPa are averaged. The surface pressure at the location of the satellite observations are used to determine the 100hPa layer.

2.2 Emission estimates tooling

The plume based fitting routine presented here was developed together with two other methods to form the core of the space-emissions tool as developed for the Umweltbundeamt (UBA). The other two methods are a simple mass-balance approach, which was coined the "naive method", and a third method, the divergence approach as described by (Beirle et al., 2016). The tooling is available in two forms, an open-access standalone offline tool, which contains all three methods and of which the source-code can be found at https://github.com/UBA-DE-Emissionsituation/space-emissions, and an online web-tool which currently only allows for the use of the naïve method. The focus in this study is on the plume based fitting method. More details on the other methodologies and inter-comparison of these (other) methods can be found in (Dammers et al., 2022b). The tool is offered as a web-based application available at: https://space-emissions.net/. The data processing is hosted at the German national Copernicus data service initiative (https://code-de.org/de/), which offers a direct link to the required Sentinel-5P data products especially tailored for governmental agencies of Germany. This web-based application tool is directly targeted at users from the emission inventory community and, therefore, uses the TEMIS monthly L3 data product available from in the naive method processing. The design of the tool is based on a modular structure that encourages later additions of other compatible air pollutants to the tool chain such as SO_2 or to add more technical and computational more demanding methods, other than

https://doi.org/10.5194/gmd-2022-292
Preprint. Discussion started: 16 December 2022

Geoscientific Model Development Discussions

the here employed mass-balance technique in later development steps. This was necessary as it offers a concise development framework to which more advanced techniques may be added later on, driven by the emission inventory community.

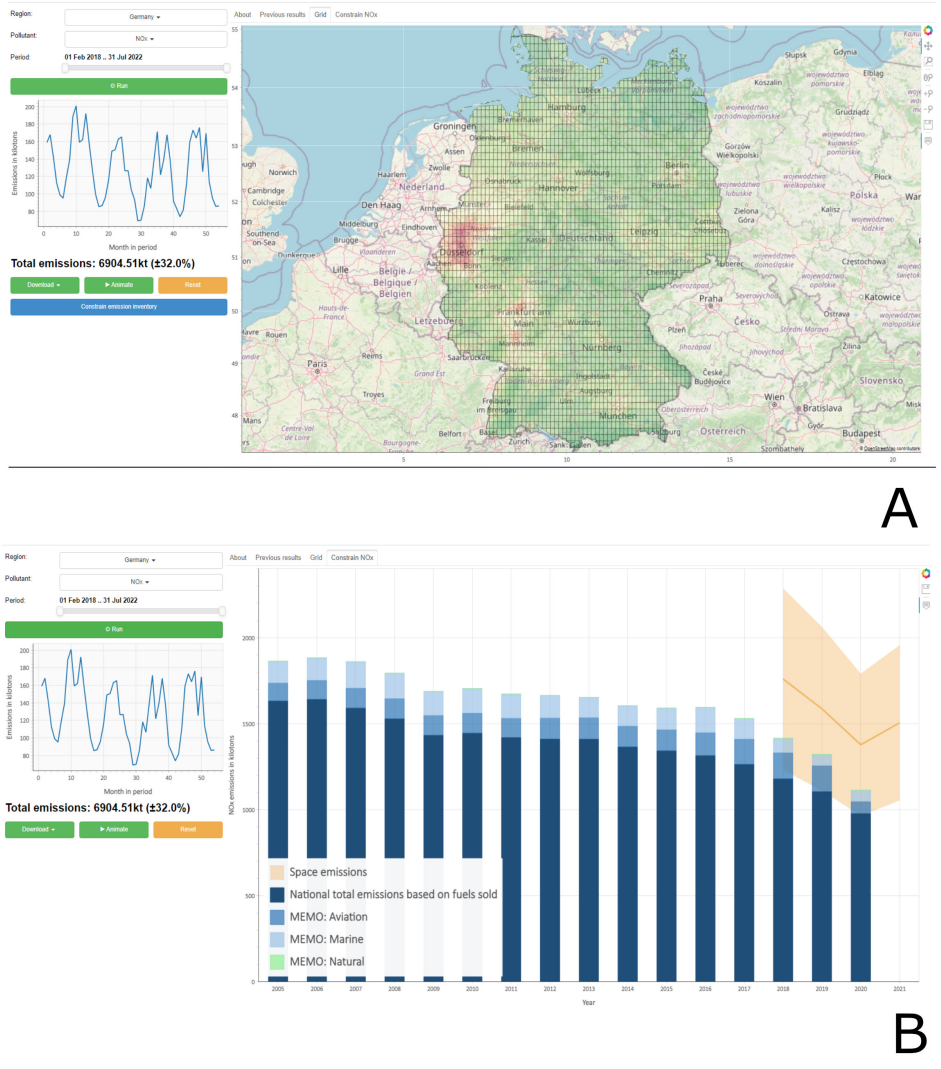

Figure 2. Screenshots from the space-emissions tool https://space-emissions.net/ for Germany. A illustrates the interface and the visualisation of the result. Whist B illustrates the result in context to the reported NO_x values.

210 The workflow of both the offline and online tools are as follows, also shown in Fig. 2: A user is required to select the country of the world they want to target with their analysis, as well as the desired air pollutant (in this case NO_2), from the respective pull down menus of the processing options (online) or by providing a shapefile of the region of choice (offline). After that, the time span for the observations needs to be selected, where data is available from the onset of the S5P NO_2 data

https://doi.org/10.5194/gmd-2022-292
Preprint. Discussion started: 16 December 2022

Geoscientific Model Development Discussions

product (February 2018). At last, the user initiates the computation, which returns the analysis results to the graphical user interface. The user may then download the graphical results as well as the analysis results as a comma separated value (.csv) file and/or other ancillary data using the post-processing options (netCDF4 files). Advanced users and software developers are also encouraged to visit: https://github.com/UBA-DE-Emissionsituation/space-emissions for the source code of the project.

2.2.1 Multi-source plume method (MSPM)

Emissions were derived using the Multi-source plume method (MSPM) (Fioletov et al., 2017; McLinden et al., 2022; Dammers et al., 2022a), which was originally developed by Fioletov et al. (2017) and can be used for an assessment of emissions from both area and point sources. For a more detailed explanation we refer readers to those publications. In short, the method relates observations and emission sources by creating a linear system of plume functions which effectively establish a system of source and receptor relations, Eq. 1, in which the total column density of each observation is described as a combination of total column densities of all sources plume functions.

$$\mathbf{A}\mathbf{x} = \mathbf{B} \tag{1}$$

In Eq. 1 **A** represent a linear system of source-receptor relations, **x** the emission sources, and **B** the satellite observed vertical column density, in our case the TROPOMI-NO_2 tropospheric columns. Several additional terms can be incorporated in **x** to account for regional product biases and for background concentrations. While the TROPOMI-NO_2 product does have local biases, the small number of validation stations hampers an accurate determination and correction for the product bias. To account for the bias we apply a correction on an overpass to overpass basis, following Beirle et al. (2016), removing the lowest 5% of the observed total column density within the larger domain. The short lifetime of NO_2 ensures that further corrections for background concentrations is not needed.

Any (Gaussian) plume function can be used to represent the relations in matrix **A**, here we use the EMG plume function, which has been successfully applied in previous studies (de Foy et al., 2014; Fioletov et al., 2017; McLinden et al., 2020; Dammers et al., 2019). Using this method observations are rotated around a single point, the emission source, so that each is positioned in a similar upwind-downwind frame (Pommier et al., 2013) with respect to the wind direction. This enables us to describe the position of each observation as a point within a downwind plume. For more details on the plume rotation method see, Fig. S4 in Pommier et al. (2013). The EMG plume function describes the vertical column density (VCD) concentrations downwind of a source. The VCD at each position x,y near a source can be described by Eq. 2, where a represents the peak enhancement, *f(x,y)* the crosswind diffusion (Eq. 3), and *g(y,s)* (Eq. 4) a convolution of the downwind advection and diffusion, within all functions, *x* the crosswind position, *y* the downwind position, and *s* the wind-speed.

$$Column_{NO_2,j}(x,y,s) = a \cdot f(x,y) \cdot g(y,s) + B \tag{2}$$

https://doi.org/10.5194/gmd-2022-292
Preprint. Discussion started: 16 December 2022


Geoscientific Model Development Discussions

$$f(x,y) = \frac{1}{\sigma_1\sqrt{2\pi}} exp\Big(-\frac{x^2}{2\sigma_1^2}\Big) \tag{3}$$

$$g(y,s) = \frac{\lambda_1}{2} exp\Big(\frac{\lambda_1(\lambda_1\sigma^2+2y)}{2}\Big) erfc\Big(\frac{\lambda_1\sigma^2+y}{\sqrt{2}\sigma}\Big) \tag{4}$$

$$\sigma_1 = \begin{cases} \sqrt{\sigma^2 - 1.5y} & ,y < 0 \\ \sigma & ,y \geq 0 \end{cases} \tag{5}$$

$$\lambda_1 = \frac{\lambda}{s} \tag{6}$$

Parameters, σ and λ represent the plume-spread and decay-rate of NO_2, with $\tau = 1/\lambda$ being the decay time or life time. The parameters σ_1 and λ_1 shown in Eqs. 5 and 6 represent the adjusted form of a plume upwind of the source (σ_1), and the the decay-rate divided by the wind-speed (λ_1). Each observation j can then be described by the sum of the enhancements of all sources i forming, Eq. 7.

$$Column_{NO2j}(\psi_j, \theta_j, \mathbf{s_j}) = \sum_i a_i f(x_{i,j}, y_{i,j}) g(y_{i,j}, s_j) + B_{i,j} \tag{7}$$

The emission rate of each source i can then be calculated by dividing the emission enhancement a_i by the decay-rate λ; $E = a/\tau = a\lambda$.

In this work a grid with a resolution of 0.1 x 0.1 degrees is used to describe the emission, covering the full domain of Germany with two degrees of padding added to the domains edges to reduce any edge effects (Dammers et al., 2022a). Following Beirle et al. (2016) we assume a lifetime of about 4 hours($\pm$25%). The plume-spread can be seen as a combination of the diffusion, satellite footprint size, and the spatial size of the sources (McLinden et al. (2022)). Taking into account the effective TROPOMI foot-print as well as the added diffusion we use a value of 7 km for the plume-spread. A dampening factor is added to the linear system in equation 1, forming Eq. 8 to reduce oscillation effects within the solution. The resulting sparse linear system can be solved efficiently with the Scipy sparse.linalg.lsqr package (Paige and Saunders, 1982; Virtanen et al., 2020).

$$\begin{bmatrix} \mathbf{A} \\ \gamma\mathbf{C} \end{bmatrix} \mathbf{x} = \begin{bmatrix} \mathbf{B} \\ \mathbf{0} \end{bmatrix} \tag{8}$$

Satellite observations of short lived species are only representative of emissions near the overpass time. A correction factor should be applied to the satellite-based estimated emissions to account for the diurnal and seasonal variability. To account for

https://doi.org/10.5194/gmd-2022-292
Preprint. Discussion started: 16 December 2022


Geoscientific Model Development Discussions

this we can use a basic box-model to approximate the mass over time and apply a posterior correction. Assuming a mass $m(t)$, and a constant lifetime ($\tau = 1/lifetime$) and E the emission at time t, the mass can be calculated with,

$$m(t) = m(t-1)e^{-\tau} + E(t) \tag{9}$$

This equation is applied to the domain-wide emissions that are injected into the domain for a whole year, including a few days of spin-up, and averaged and normalised for a selection of expected lifetimes. For the temporal distribution we use the average NO_x emission profile for all NO_x sources within the German domain as used in the LOTOS-EUROS model (Manders et al., 2017). A lifetime of about 4 hours and an overpass time of around 13:00 LST results in a correction factor of 1.24, meaning that the estimated emissions can be expected to bias high by around 24%.

Depending on the source location and time of year this value is expected to vary due to variations in the temporal emission profile. However, as actual measurements of diurnal cycles of nitrogen-dioxide emissions are rare and only exist for larger power-plants, only the variability in the model emissions can be used to create a regional adjustment parameter. Surface concentration observations should in turn be used to analyse and optimize the modelled diurnal emission profiles for individual sectors. To calculate the viability of such a regional factor the adjustment parameter was calculated for each cell. The standard deviation of the regional parameters is around $\sim$0.05. Therefore, to reduce complexity, the value of 1.24 is assumed for the entire domain. A similar parameter is derived to account for the seasonal variability of the emissions in combination with the variable availability of TROPOMI-NO2 observations passing the data quality filters. The correction parameter is calculated as the weighted mean of the number of observations per month and the mean correction factor for each month. Using this approach a value of 1.05 is found. Combined with the diurnal parameter this gives a factor of approximately 1.30.

TROPOMI is only capable in observing NO_2, therefore an additional correction is needed to account for the NO mass. In previous studies this is commonly done by using a NO_x/NO_2 concentration ratio. Values commonly lie within the 1.3-1.4 range (Beirle et al., 2011, 2016) depending on the local chemistry. In this study we apply the 1.32 factor as used by Beirle et al. (2016).

2.2.2 Sector specific emissions

A direct sector based attribution of emissions is not feasible using the satellite data only. Therefore, additional data needs to be taken into account to attempt to estimate a potential sectoral attribution of the emission. We used the GNFR/CLRTAP sector outputs to create a spatial index filter for the emission data. The gridded NFR data is used as a basis and summed to the 0.1°x0.1° grid for each of the NFR classes. A Gaussian filter (*scipy.ndimage*,Virtanen et al. (2020)) is applied to the data with a sigma of 1 grid cell, applying a light smoothing to account for the maximum resolvability of each source and emission methodology. The resulting masks are divided by the total emissions of all sectors to derive each sector's fraction of all emissions (emission fraction), and shown in the supplement Fig. A1 for the non smoothed version and Fig. A2 for the Gaussian smoothed version. For further sectoral emissions analysis only locations with an emission fraction above 50 % are selected, the resulting mask is shown in Fig. A3.

https://doi.org/10.5194/gmd-2022-292
Preprint. Discussion started: 16 December 2022


Geoscientific Model Development Discussions

3 Results

3.1 Inter-comparison with the emission inventory

For a comparison with the gridded inventory data, we used the 2019 data from the satellite derived emissions and the respective NO_x data from the GNFR inventory (CLRTAP, 2021). Figure 3 gives a visual comparison of the 2019 data sets. Both sets were compared using the Structural Similarity Index Measure (SSIM) (Wang et al., 2004) for a quantitative comparison of the images. The SSIM operator is a metric, which was developed to evaluate the image quality of video frames . It uses a window based comparison analysis to track subtle differences between two images so that the spatial structure of both images is also taken into account when calculating the SSIM score. This way similarity and dissimilarity between two 2D data sets may be quantified with the SSIM score in a way, which assesses image similarity in a more human-vision-based mode. Since its introduction SSIM has become a standard comparison operator for computing the similarity between 2d data sets and is now also available in standard open-source data analysis packages such as scikit-image (van der Walt et al., 2014).

The resulting SSIM analysis for the 2019 GNFR and TROPOMI derived emission data shows a SSIM score value of 0.6 between both data sets. However, to consider the different approaches of both data sets and to harmonize effects of different baseline resolution, a Gaussian filter is applied to both sets of data that compensates the effect of the larger point spread function (PSF) of the sensor. If both images are Gaussian filtered and compared the resultant SSIM score is 0.79 and now closer to a score of 1.0, which would depict spatial structure identity between the two sets of data. This illustrates that the spatial structure of both data sets show a high similarity and space-borne derived emissions from the method presented here capture similar large emission sources such as major cities, road networks and industrial areas as the GNFR data set.

3.2 Multi-year emissions

The satellite derived emissions for the individual years between 2019-2021 are shown in Figure 4. The rightmost plot shows the emissions as part of the GNFR inventory emissions. A comparison between the satellite derived emissions of individual years and the inventory emissions for 2019 are shown in Fig. 5. Figure 6 shows the change in the spatial satellite derived emission distribution of the largest sources in Germany between 2019 and 2020 or 2021. As the gridded inventory emissions are only available for 2019, we can only compare the individual years to that years inventory emissions.

Fig 4 again illustrates the exceptional qualities of the TROPOMI instrument over previous sensors. Fig 4 shows that the spatial data from the 2019 space-borne emission estimates have elevated NO_x emission values of around 5-7t/km^2 outlining the major motorway network in Germany. Most notably is the motorway A2 westwards from Berlin, via Magdeburg and Hannover towards the Rhine-Ruhr region. Another interesting motorway is the A1 from the Ruhr area of North-Rhine-Westphalia towards Bremen and Hamburg. The motorway ring and spider-alike road networks and settlements fanning out from around Berlin are also nicely visible in 2019.

While the TROPOMI instrument represents a huge step in the capabilities to spot individual emission sources, there are still limits to the spatial resolvability. The top row of Fig. 5 shows a direct comparison while the bottom row shows the same results but now with the application of the Gaussian filter, as previously used in Fig.3. The main difference between these

https://doi.org/10.5194/gmd-2022-292
Preprint. Discussion started: 16 December 2022

Geoscientific Model Development Discussions

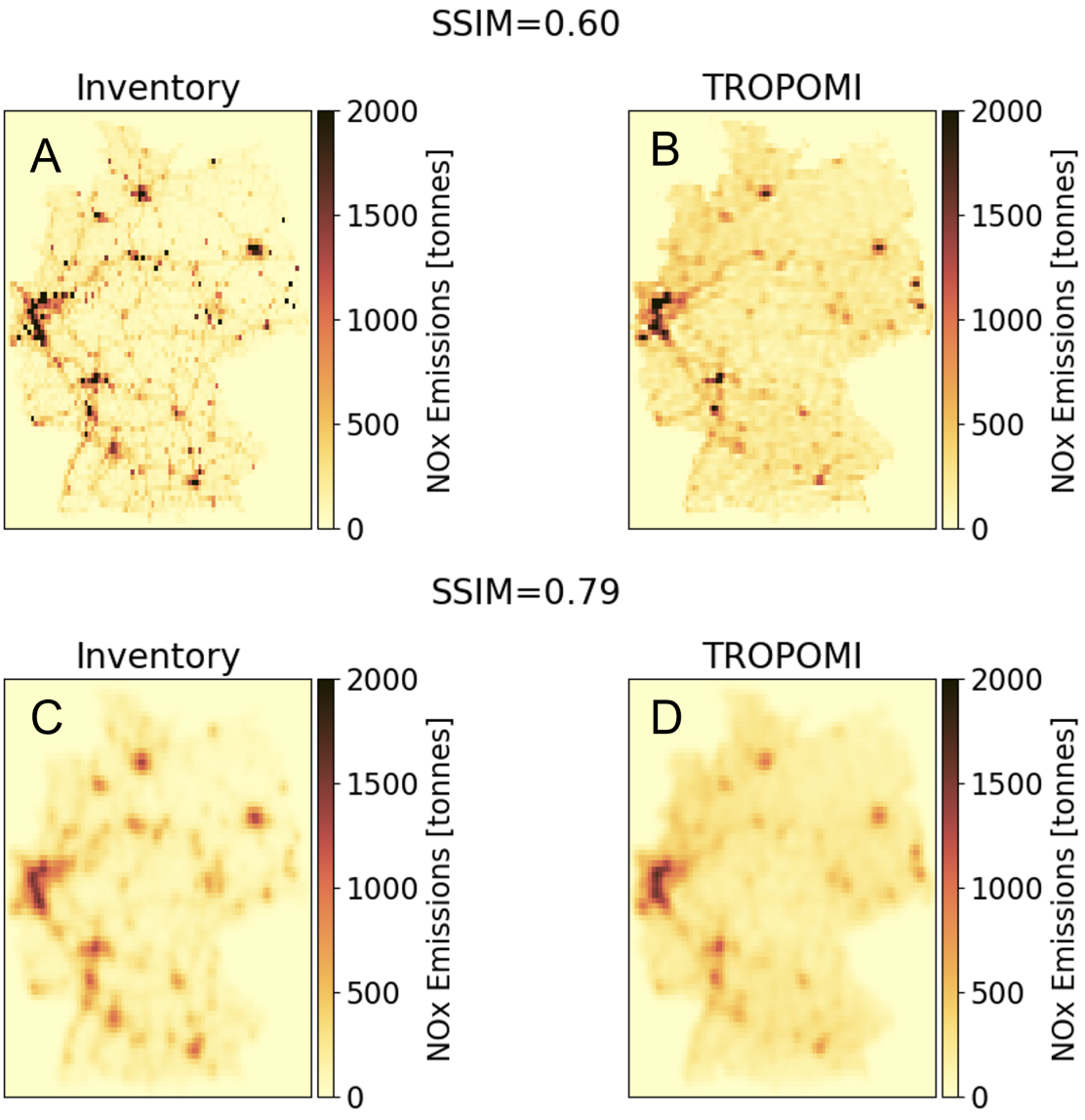

Figure 3. The Structural Similarity Index Measure SSIM of 0.6 was calculated between the gridded inventory data (top-left panel, A) and the emissions derived with the TROPOMI data for 2019 (top-right panel, B). Please note that the details in the (image-) data structure (major road networks and urban areas) are very similar between both sets of data. This is highlighted by a SSIM score of 0.6, which quantifies as the similarity between the data as highly significant. If the data is Gaussian filtered effects of spatially sharper GNFR data(panel C), compared to TROPOMI data (panel D) are compensated and yield a SSIM score of 0.79

https://doi.org/10.5194/gmd-2022-292
Preprint. Discussion started: 16 December 2022

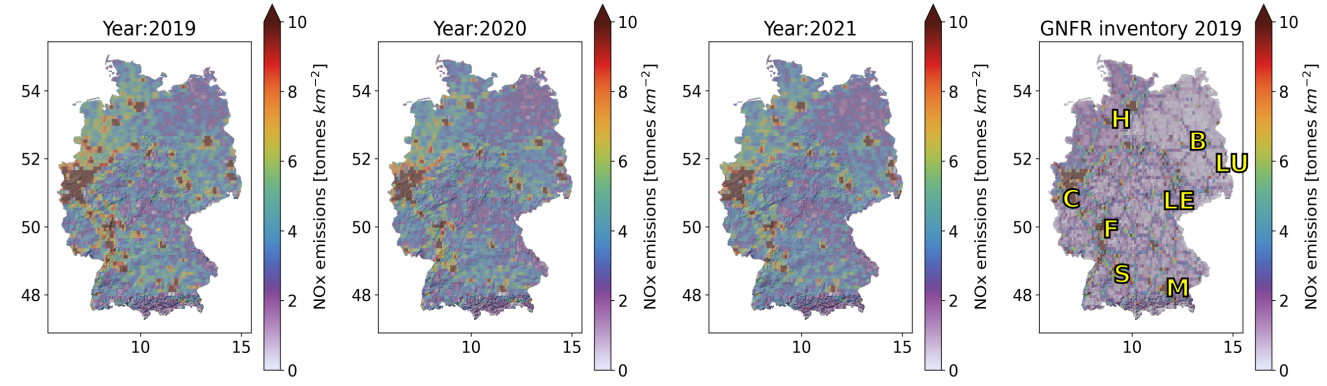

Figure 4. From left to right; NO_x satellite derived yearly emissions for 2019-2021, and the GNFR inventory emissions of 2019. Rightmost figure H: Hamburg B: Berlin, C: Cologne, LU: Lusatia, LE: Leipzig, M: Munich, S: Stuttgart, F: Frankfurt.

two rows are the large positive/negative swings around the more localized emissions and/or major point source like emitters such as power-plants. Such variations are however not observed around emitters with a large spatial footprints such as cities. This is an excellent showcase of the limit of the method and satellite instrument. Through the size of the satellite pixel's footprint and the misrepresentations of the wind fields (i.e. artefacts) there is an actual limit to the overall spatial resolvability of individual sources. This limit was reported by McLinden et al. (2022) to be around 5-10km for TROPOMI, which matches well to the size of the source grid used here. The 0.1x0.1 degree spatial resolution used in this study is thus at the limit of the methods capabilities to constrain individual neighbouring sources and some smearing is thus expected around the strongest point like sources. The Gaussian (smearing) filter can be used as a first order correction, which results in the lower row of plots. Compared to the inventory emissions of 2019, the Figs. 5 D, E and F show similar patterns between the years, with strong negative differences observed around the major sources, while the background regions (i.e. regions with emissions below 2 tonnes km^2) show a consistent positive difference of around 0-1 tonnes km^2. There are several potential causes for these systematic patterns which will be evaluated in the discussion section.

Outside of the systematic patterns there are several variations visible between the years. The year 2020 shows a noticeable drop in NO_x emissions around the before mentioned industrial, cities, and highways (Fig. 6). The largest reduction of NO_x emissions between 2019 and 2020 are in the industrial areas in the Rhine Ruhr region and the upper Rhine area. The rise in emissions from 2020 to 2021 in the TROPOMI data in Fig. 4 and Fig. 6 is most noticeable in the larger urban areas. However, the 2021 NO_x emissions are still lower than in 2019, for example in the industrial centers of the Rhine-Ruhr region (note the red dots indicating the major industrial emitters) and further south along the Rhine. Only the A1 motorway is still clearly visible in the 2020 and 2021 emission estimates (Fig. 4), whilst the data from other settlement and road networks (e.g. around Berlin) is much less obvious than in the 2019 emission estimates. This is also visible in Fig. 6 in the area with roads leading

https://doi.org/10.5194/gmd-2022-292
Preprint. Discussion started: 16 December 2022

Geoscientific Model Development
Discussions
Open Access
EGU

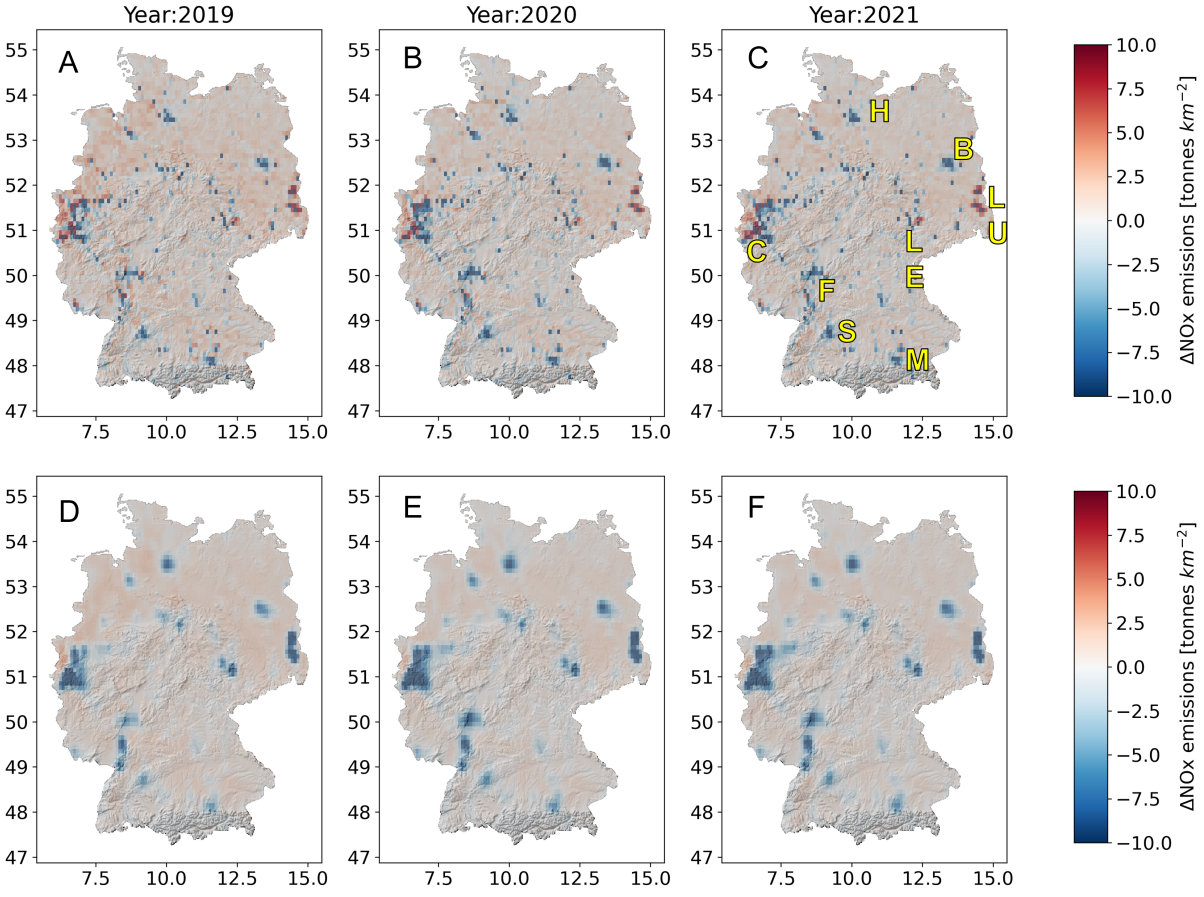

Figure 5. Difference between the satellite derived and inventory emissions (2019) for years 2019-2021 (A-C). Top row shows the original difference between both emission sets, the bottom row shows the same sets but now with the Gaussian filter applied to both sets before subtracting the 2019 inventory emissions (D-F).

away from Berlin, where the difference between the 2021 and 2019 estimated emissions still show negative difference of the order 0-1 tonnes km^2.

Two of the most prominently visible changes (2019-2020) shown in Fig. 6 are the industrial "Ruhr" region, the largest and oldest industrial core of Germany in the westernmost part of the country, and the area of Lusatia in the eastern part of the country with its big lignite mining for power generation in coal fired power plants. These two areas are shown as detailed maps in Fig. 7. Compared to 2019 the emissions have dropped substantially in 2020 and 2021 (up to <-5t/km^2). The power generation in Germany has seen an upsurge in the usage of coal fired power stations for power generation in 2021 compared to the COVID-19 year 2020, as reported by the DESTASIS in its press briefing (link) stating that coal had been the most important source of electricity generation in Germany in 2021. This can be seen in Fig. 7, where there is an increase near one of the large

https://doi.org/10.5194/gmd-2022-292
Preprint. Discussion started: 16 December 2022

Geoscientific Model Development Discussions

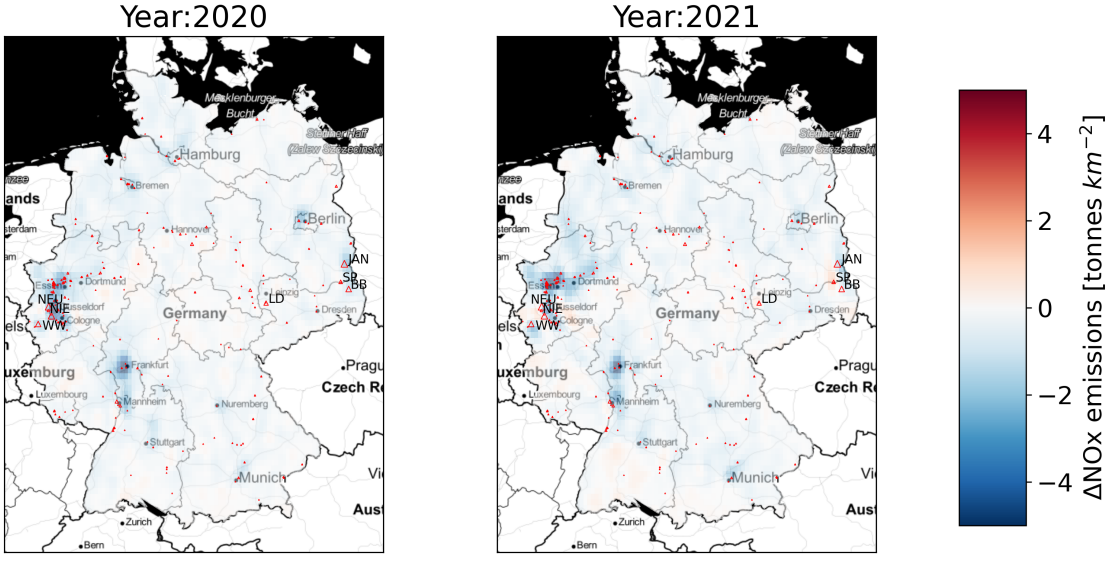

Figure 6. Difference between 2020-2019 and 2021-2019 satellite derived emissions. A Gaussian filter has been applied to both derived emission sets. The red dots indicate the locations of the largest NO_x emitters within Germany, with the size of the dots a reflection of the individual source strength.

emission centers right at the eastern border of Germany. The Schwarze Pump (SP) and Lippendorf (LP) power-plants even show an increase in emissions compared to 2019. Meanwhile the emissions from the Janschwalde (JAN) power-plant show a strong reduction in 2020 that continues into 2021, which was expected as the power-plant reduced its operation capacity as planned (Vattenfall, 2015; EPH, 2022). The three large power-plants in the west show similar patterns with the Neurath (NEU) and Niederaussem (NIE) plants showing a strong decrease in 2020 rebounding upwards moving into 2021. The Weisweiler power-plant reduces into 2019 while reducing further into 2021. This drop can be explained by two potential causes. Firstly, a reduction of operation capacity was planned. and secondly by the floods caused by exceptional rainfall in mid July 2021, which also affected the nearby lignite mining pits (RWE statement / Link to news item).

3.3 Sector-specific emissions

An aggregated version of the spatially distributed results is shown in the bar plot of Fig.8, in which the country wide fitted emissions are compared to the country-wide sector specific emission totals. Note, that we added the 60kt from natural soil emissions and 5kt from lightning emissions to the N_Natural class. These emissions were not included in the previous spatial plots. In line with the previously discussed results, both the satellite and inventory emissions show a large drop from 2019-2020, of comparable size. The slight increase in the projected inventory emissions from 2020-2021 is however not matched by a

https://doi.org/10.5194/gmd-2022-292
Preprint. Discussion started: 16 December 2022

Geoscientific Model Development
Discussions
Open Access
EGU

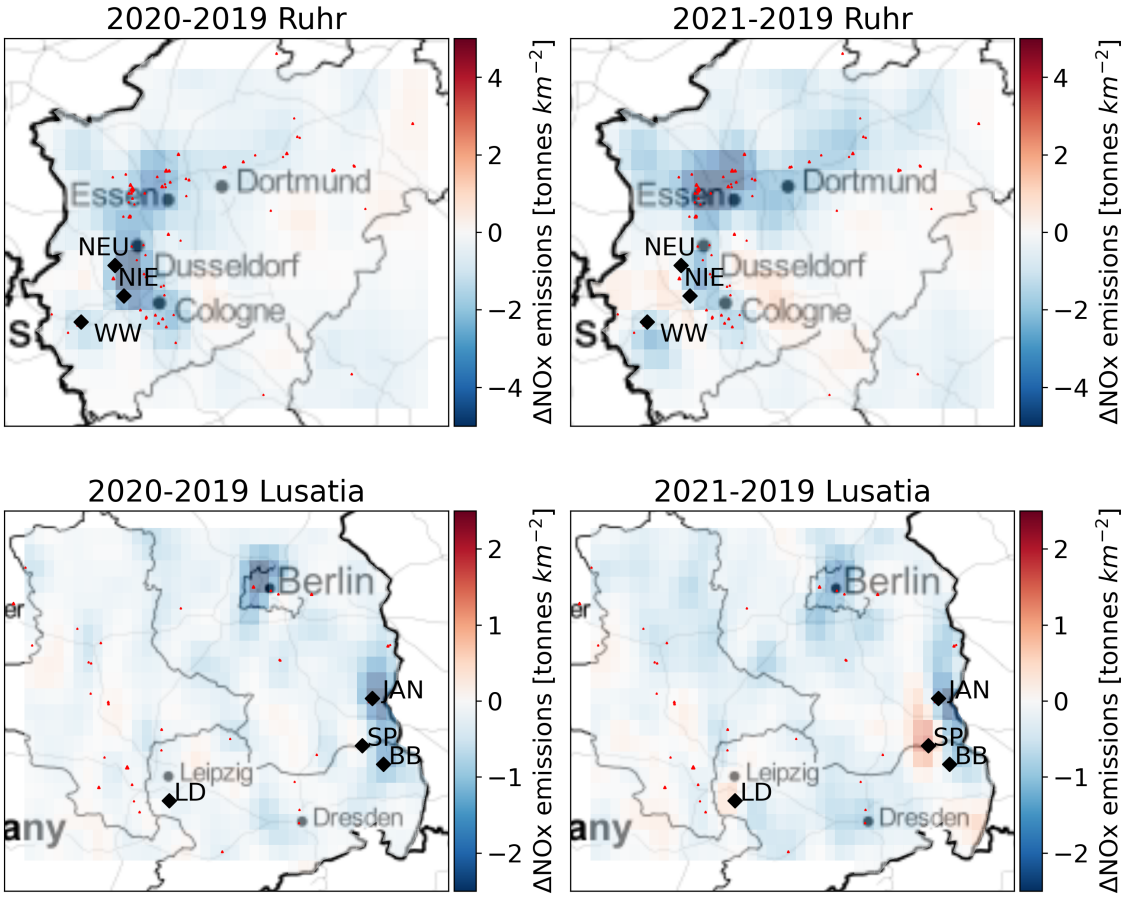

Figure 7. Difference between 2020-2019 and 2021-2019 satellite derived emissions. Upper row depicting the industrial "Ruhr" region, whilst the lower 3 panels show Lusatia at the eastern border of Germany. A Gaussian filter has been applied to all data sets prior to subtraction. The red dots indicate the locations of the largest NO_x emitters within Germany, with the size of the dots a reflection of the individual source strength.

https://doi.org/10.5194/gmd-2022-292
Preprint. Discussion started: 16 December 2022

Geoscientific Model Development Discussions

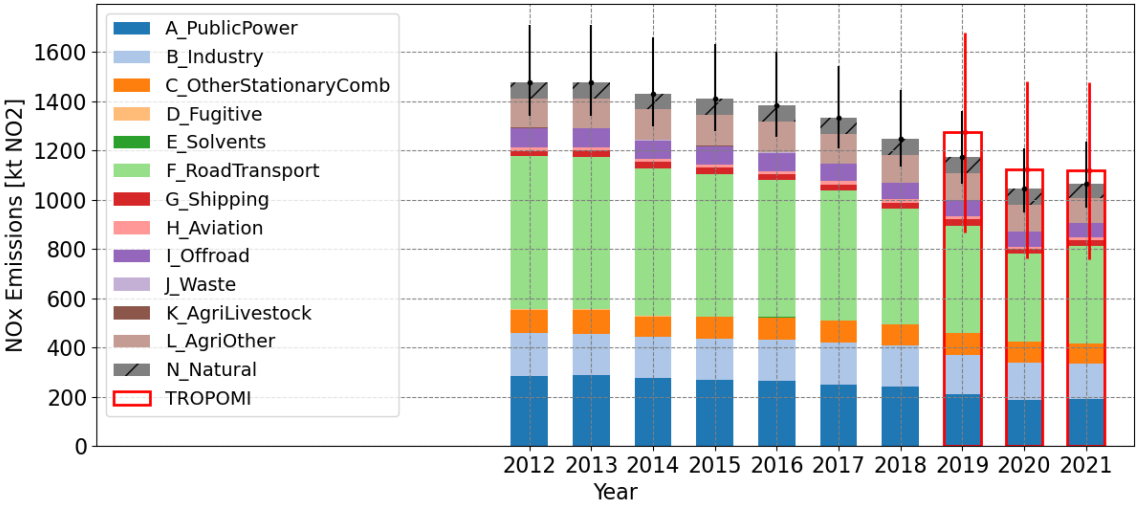

Figure 8. Emission changes over the years as reported by the national inventory of Germany and observed by the TROPOMI instrument. Note the slight rise in 2021, compared to the year 2020 due to COVID-19 lockdown measures.

change in the satellite emissions. Emissions sources that have a strong spatio-temporal imprint on TROPOMI data should show independent patterns for regions where the sources cause the majority of emissions. To find out what type of source is causing this mismatch, we make use of the sectoral masks (e.g. fig. A3) to derive sector specific patterns from the spatio-temporal data from the satellite derived and inventory emission data. Only 5 sectors have locations which are dominated (e.g. above 50% of the total emissions) by a single emission sector, of which the PublicPower sector has the largest emissions in a single location while the road transport and agricultural emissions are more spread out over roads and pastures throughout the country. Note, that the PublicPower, Shipping and Industrial emissions cover a very limited area with only PublicPower showing very high emissions. Figure 9 shows the sector specific emissions as indexed by the 2019 emissions for the non-agricultural sources. Based on earlier projections, and trends over the previous years, 2021 inventory emissions are expected to be at just over 90% of the 2019 emissions. The emissions related to power generation have bounced back almost to the pre-COVID levels even though the Janschwalde power plant in the east reduced its operation capacity as planned (Vattenfall, 2015; EPH, 2022). Further resurgences are to be expected (for 2022) by the plans of the reactivation of old coal fired power plants in the wake of the European energy crisis and the potential fears of a blackout in Germany. While Road transport emissions were expected to show a recovery this is not matched by patterns in the satellite derived emissions. The slow recovery can potentially be explained by the reduced number of kilometers by trucks (>3500kg) which is almost down by 10% in 2021 compared to 2019 (KBA, 2022). Shipping emissions have continued their trend with no show of any recovery. While this reduction was expected based on past trends, the cause can be found in the global shipping crisis and disrupted supply chains.

https://doi.org/10.5194/gmd-2022-292
Preprint. Discussion started: 16 December 2022

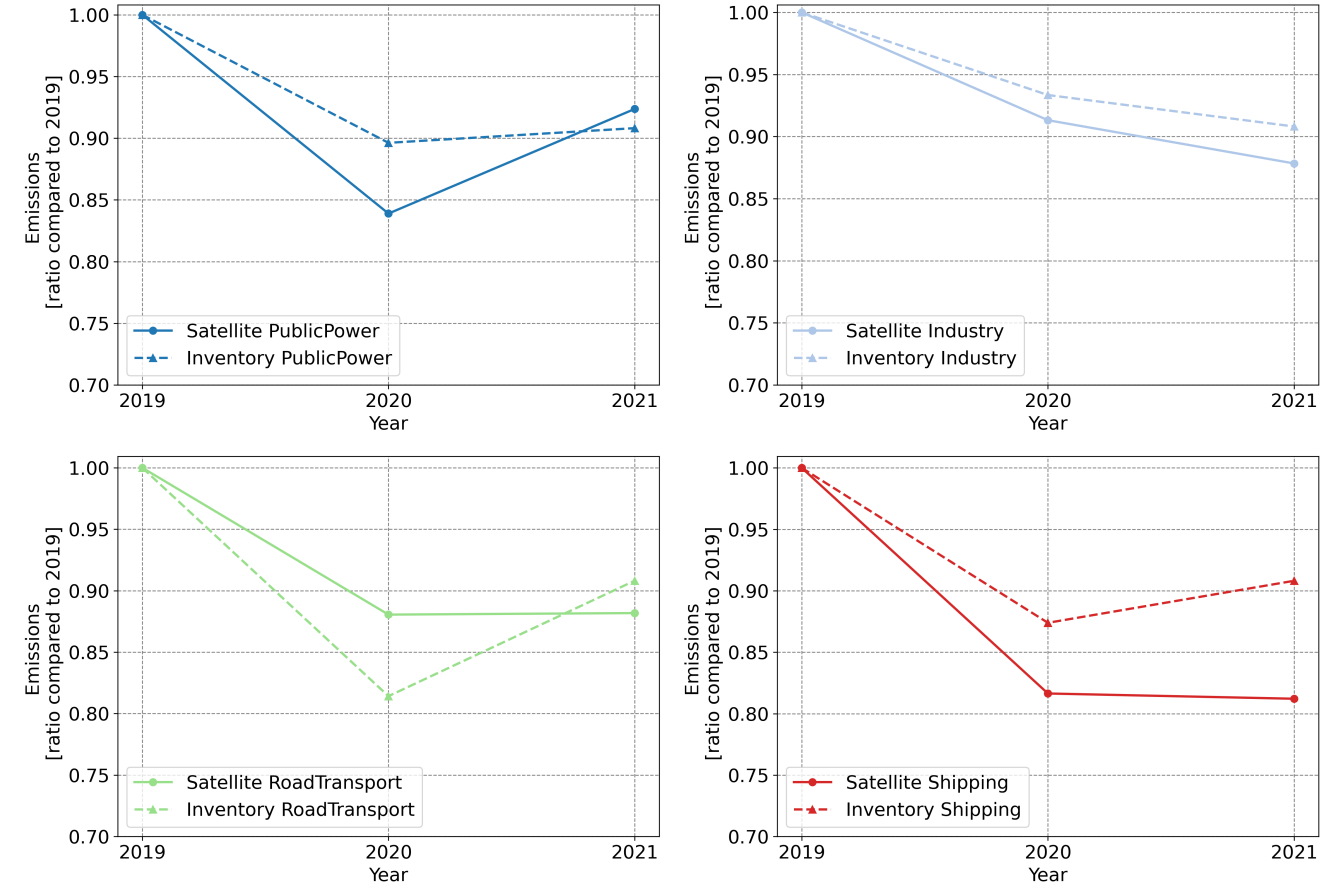

Figure 9. Satellite derived and inventory emissions for each source sector as indexed by the 2019 emissions. A clear downward trend is visible for most sectors. Dotted lines indicate the inventory emissions, the other line the satellite derived emissions.

https://doi.org/10.5194/gmd-2022-292
Preprint. Discussion started: 16 December 2022


Geoscientific Model Development Discussions

4 Discussion

As the results showed, the captured spatial variability within satellite derived emissions are very similar to those in inventory emissions. The values for the NO_x emissions retrieved from the TROPOMI observations diverge on average 100kt from the reported emissions. There are some variations observed between the years but the difference between both series fall within the uncertainty range of both emission totals (Fig. 8). The uncertainties of both sets are quite large compared to the yearly variations, which hampers stronger conclusions on the quality of the inventory and satellite based estimates. We can however discuss the various causes of uncertainty and how these can be reduced. The uncertainty range of the reported inventory emissions is estimated to fall between -9.2 and +15.8% (see https://iir.umweltbundesamt.de/2022/), which translates to about -100 to +180 kt in 2019 for the inventory. Note that this range does not include potentially missed sources, such as stronger than expected natural emissions and any of the MEMO items. As discussed in section 2.1.1 especially soil emissions show large range within the literature, and some of the spatial patterns show possible hints a smaller but widespread source throughout Germany (Fig. 5). Besides the above discussed items it should be noted that the emissions from road transport are required to be based on the fuels sold approach. This approach does not account for all the emissions which occur in Germany from vehicles which were fueled abroad and are driving in Germany (this might constitute an underestimation in the inventory). On the other hand the emissions from foreign vehicles (for instance from the Netherlands) which bought their fuel in Germany and were not driving in Germany are in this fuel sold approach allocated to Germany (this might constitute an overestimation of the German emissions). However it is not known how much emissions are associated with these cross border phenomena's for Germany. Data from The Netherlands show this might be a significant difference; the NOx emission based on fuel used is approximately 5.5 % less than the emissions based on fuel sold as reported in the GNFR total. However as fuel prices in Belgium and Germany are cheaper than in The Netherlands, Dutch drivers fuel frequently in those countries thus the Dutch case represents the higher end of the difference between fuel sold and fuel used approach, only surpassed by Luxembourg with one of the lowest fuel prices in Europe. Another source of uncertainty are the emissions near the border regions. Emissions within the first 10 to 20km outside of the border can be expected to be smeared out in the inversions due to the limited resolvability of the instrument and methodology. The stronger the source is, the better is the resolvability. So for the larger sources 10 km can be assumed. Making a loop around the German borders there are a few areas of interest. Starting at the border of the Netherlands and moving clockwise on both sides of the border, there are several larger sources, such as the Weisweiler power plant in Eschweiler, the Dolna Odra power station in Poland, and several power plants near the border in the Czech Republic, but also several smaller and larger cities. By taking a polygon that is 10 km wider and narrower in shape than the existing German borders the smeared emissions near the borders can be approximated. Based on the European CAMS-REG v5.1 inventory (emissions 2018, based on the in 2020 reported emissions, (Kuenen et al., 2022)) we find that around 120 kt of the German emissions take place within Germany and within 10 km of the borders, and around 75 kt just outside of Germany within 10 km of the border. Assuming that at most half of the full amount of these emissions smear out past the border, the smeared loss in emissions is about 22kt on the total emissions. This should be seen as an upper limit. Furthermore, of these

https://doi.org/10.5194/gmd-2022-292
Preprint. Discussion started: 16 December 2022


Geoscientific Model Development Discussions

emissions a large majority takes place in the western part of Germany, where the most common wind direction is wind coming from the west. In effect it can be expected that the smearing of those emissions will be reduced further.

A more probable source for the 100kt mismatch however can be found in the satellite derived estimates. The TROPOMI based emission estimates on average have an uncertainty in the range of 30-40% translating to about +-400kt and based on various uncertainty parameters. Based on the multi-source methodology we can point out several important parameters of uncertainty. Firstly, there is the TROPOMI-NO_2 product. As stated earlier, the current TROPOMI-NO_2 product overestimates concentrations in background/low emission regions (+a few %) while having a negative bias in source regions (-35%, up to -50% in extreme cases (Verhoelst et al., 2021), although improved from a mean bias of around -32% to -23% (van Geffen et al., 2022)). The cause for the bias can be found in the inaccuracies of the air mass factor (AMF) which comes from uncertainties in the underlying modelled concentration fields and missing variations in the stratospheric NO_2 concentrations. Local variations due to errors in the AMF cannot be corrected for without the use of a chemistry transport model (CTM) and can lead to under and overestimation of emissions in high source and background regions. A recent approach u using the modelled CAMS-Europe profiles show that the large negative bias can be resolved with the help of higher resolution a-priori profiles. Beside this systematic uncertainty the VCDs will also have a random uncertainty, but due to the large number of observations used to constrain each source, the impact of those uncertainties is expected to be minor. Finally, there is the detection limit of the TROPOMI instrument, which limits the detect ability of sources. The study by Beirle et al. (2016) gives a limit of about 0.11kg/s, although based on the Divergence method. An emission source of 0.11kg/s equals about 3.5kt NO_x per year. This is based on a peak fit which typically has a radius of 25km, which roughly gives us a 2500km^2 area, which when dividing the detection limit over the area, results in an detection limit of around 1.4 tonnes km^{-2}. To put that number in perspective, the smaller differences observed in Fig 5 are in many cases above that limit except for the background regions in southern Germany. Secondly, while the assumption of a 4 ($\pm$25%) hour the effective lifetime seems to be correct for 2019 Germany as a whole. It is important to note that an underestimation of the chemical losses could lead to an overall overestimation of the emissions, and vice versa an overestimation of the lifetime can lead to an underestimation of the emissions. A doubling of the lifetime roughly halves the emissions which shows the importance of the parameter. Lifetimes however are location-dependent and require more detailed plume and chemistry studies. Examples of recent other studies show the large ranges for the NOx (chemical) lifetime. Examples are the study by Lorente et al. (2019) give a range of 11 hours in winter, to 1-4 hours in spring for the region around Paris. Previous studies specifically using the EMG plume function found effective lifetime in the order of 2-5 hours for very strong emitters. Furthermore, other possible causes for the over or underestimation of derived emissions are the diurnal and seasonal variations (expected to be several % for the seasonal variations). Currently a fixed parameter was determined for the whole German domain, but locally the diurnal correction factor can be lower for the more continuous emissions, for example in the case of power-plants, and thus in effect create a negative bias for emissions. The NO_x to NO_2 ratio can also have local variations, which affect the total emissions. For the majority NOx seems to be emitted as NO, which is then rapidly turned into NO2 after which an equilibrium is reached, of which the speed depends on the availability of O3. Beirle et al. (2021) recently gave a modelled estimate of the ratio, which was very close to the factor 1.32($\pm$20%) given in his original study, with values moving towards 1.0 for industrial areas just north of the equator while values tended towards higher

https://doi.org/10.5194/gmd-2022-292
Preprint. Discussion started: 16 December 2022


Geoscientific Model Development Discussions

ranges (1.6) for less industrialized and high-latitude regions. Finally, there is the influence of the wind fields, for which we estimate an uncertainty of up to 1m/s over flat to 2m/s in mountainous and hilly areas. The effect can move in both directions and translates into an uncertainty of around 15-20% for average conditions over Germany (based on the matched wind-fields). Taken together, these error terms result into a Germany averaged error range between 10-30% for the Gaussian plume method. The low error estimate corresponds to source regions where the low bias of the TROPOMI VCDs, effectively low biasing the emissions, are counteracted by the potentially high bias in the emissions of the NOx:NO2 ratio and effective lifetimes. Both values should be seen as conservative estimates, which would occur in the extremely unlikely case that the inaccuracy in NO_x:NO_2 ratio, lifetime, AMF and wind-fields all nudge the estimate in the same direction for all locations in the domain of interest. In reality not all errors point in a similar direction, with the AMF/concentration term pointing in opposite directions for background and source regions. A complete error analysis based on simulated observations with controlled conditions and a subsequent Monte-Carlo analysis of error propagation can give a more accurate estimate, but that falls outside of the scope of this study.

The year to year variations in the TROPOMI-NO_2 derived emissions are of the order of a few to ten % (8). While the estimated errors of individual years are larger than those variations most error components will point in similar directions between the years. For example the negative bias in the TROPOMI product can be expected to stay stable between the years over the high VCD regions while staying slightly positive over background regions. The only terms that are expected to change are the NO_x:NO_2 ratio, the effective lifetime, and changes in wind-patterns. The changes in wind-patterns will only matter for regions in the border regions as misinterpretation of the wind-fields will typically results in the wrongful attribution of emissions within Germany. These leaves the NO_x:NO_2 and effective lifetime as the main source of uncertainty, both related to the timing of emissions and the chemistry. A potential method to constrain this effect is performing a CTM run over the same period but with fixed yearly emissions over the whole period. The emission estimate methodology of this study can then be used to estimate the emissions of the individual years and thus derive the influence of changing chemistry and meteorology. This however again falls outside of the scope of this study.

5 Conclusions and Outlook

This work has shown that TROPOMI can be used as a verification tool for emission inventories, even for those inventory compilers, which are unfamiliar with remote sensing data, given the here presented web-tool. Emission inventory compilers may monitor near-real-time trends in NO_x emissions with the tool via top-down space-borne data without the need to wait for the completion of the statistical data required for the classic statistical "bottom-up" approach for the calculation of emissions. This is of particular importance for the quantification of unforeseen events such as the outbreak of the COVID-19 pandemic, which has been shown in this paper by comparing the 2019 emission data to the COVID (2020) and post-COVID year (2021). Individual sectors are, however, difficult to assess given the low spatial resolution of TROPOMI. However, if we look at single large contributors to emissions such as the public power sector shown in Fig. 9 it is possible to track the rebound in emissions after the corona year 2020. Which has been due to the increased usage of coal fired power plants for power generation in 2021

https://doi.org/10.5194/gmd-2022-292
Preprint. Discussion started: 16 December 2022


Geoscientific Model Development Discussions

compared to 2020. Similar trends and changes in NO_2 concentration may now be assessed by the emission inventory community worldwide as they are now able to compare their countries results to others using the here presented fully transparent methods. This has previously not been possible in a convenient way for inventory compilers. As at least comprehensive data science knowledge is required to access and query other data products e.g. from the ECMWF atmospheric data store (ads), the web tool is complemented by the source code offer, which specifically invites other developers to extend the space-borne emissions code-base and web-tool by their own contributions. This truly offers a substantial value to the international emission inventory community. Space-borne data from TROPOMI and other satellites contain valuable information that can be used as a verification tool for emission inventories. NO_x retrievals from space-borne sensors such as OMI and TROPOMI can be used to monitor the quite dramatically decreasing evolution of NO_x emissions over the years with new emission estimation methods such as (Fioletov et al., 2017). Although, sub-sector and facility related data still is difficult to assess, given the 3.5x5.5km^2 resolution of TROPOMI, the data still delivers valuable insight into the coarser spatial distribution of emission clusters, such as the chemical industry parks around Halle and Leipzig or large coal fired power stations in the east of Germany. This may help to monitor emission reductions directly of these large industrial clusters. This satellite-based emission estimates , based on a single consistent methodology applied to several countries, can be used to verify the compliance towards meeting the air pollution reduction targets throughout the whole of the European Union, which ensures a maximum of transparency for all stakeholders. This ultimately values the principals of the European Green Deal initiative, which tries to leverage new technology for a sustainable EU. With the presented space-emissions tool other emission inventory compilers without remote sensing expertise are encouraged to employ space-emissions for verification of their inventories. This would make the space-emissions tool a critical building block of emission compliance reporting thanks to the Copernicus Sentinel data set (i.e. TROPOMI) that are provided by ESA. We are looking forward to the feedback from the emission inventory community and their results using the online and offline tools. While the here developed methodology and online (and offline) tool is focused on NO_x emission estimates from TROPOMI observations. In future the incorporation of OMI data would also extend the time series to the year 2005, which is of great importance for the verification of a more complete time-series of the inventory. The additions of other pollutants should also be envisioned for future work under the reservation that the respective method is applicable to the selected pollutant. In the near future the geostationary Sentinel-4 satellite is scheduled for launch and will provide hourly data on tropospheric constituents over Europe. This will allow tooling such as those used in this manuscript to explore additional functionality such as the measurement of time profiles and might allow for emission estimates on a weekly of even daily basis and provide information on the diurnal emission cycle. While the methodology was only applied on a yearly basis in this study, TROPOMI has enough spatio-temporal coverage to move to seasonal or monthly estimates, potentially trading the spatial resolution of the emission fields for an increase in temporal resolvability. Future improvements to the methodology should focus on updating the AMF with the help of higher resolution modelled fields, the addition of a location dependent lifetime (for example based on concentration of NO_2, O_3 and OH), the addition of local NO_x:NO_2 ratios and local corrections for diurnal and seasonal cycles) which all three would make sense from a physical perspective and form the largest uncertainty in the method outside satellite bias. Some of these improvements require simulated model fields, of which some are available in the form of (open-access) CAMS ensemble runs (link website, model fields). Other required variables such as temperature,

https://doi.org/10.5194/gmd-2022-292
Preprint. Discussion started: 16 December 2022


Geoscientific Model Development Discussions

UV radiation, precipitation and humidity, which would be used for adjusted lifetimes, are also available at the various ECMWF data storage. These quantities and/or estimates can be downloaded with the ERA download tool and already make a relatively easy improvement to the lifetime estimates and thereby reduce the overall uncertainty of those terms.

Code and data availability. An offline version of the emission code is available at https://github.com/UBA-DE-Emissionsituation/space-emissions. All code used to produce further results figures etc, can be provided on request. The TROPOMI L2 data product versions (OFFL / PAL) can be accessed through the ESA Sentinel-5P data hub (https://s5phub.copernicus.eu) and the PAL data-portal (https://data-portal.s5p-pal.com/). The emission inventory datasets can be accessed via https://iir.umweltbundesamt.de/2022/, and the GNFR/NFR data sets via Link to NFR and Link to GNFR.

Appendix A: Additional figures

https://doi.org/10.5194/gmd-2022-292
Preprint. Discussion started: 16 December 2022

Geoscientific Model Development
Discussions
Open Access
EGU

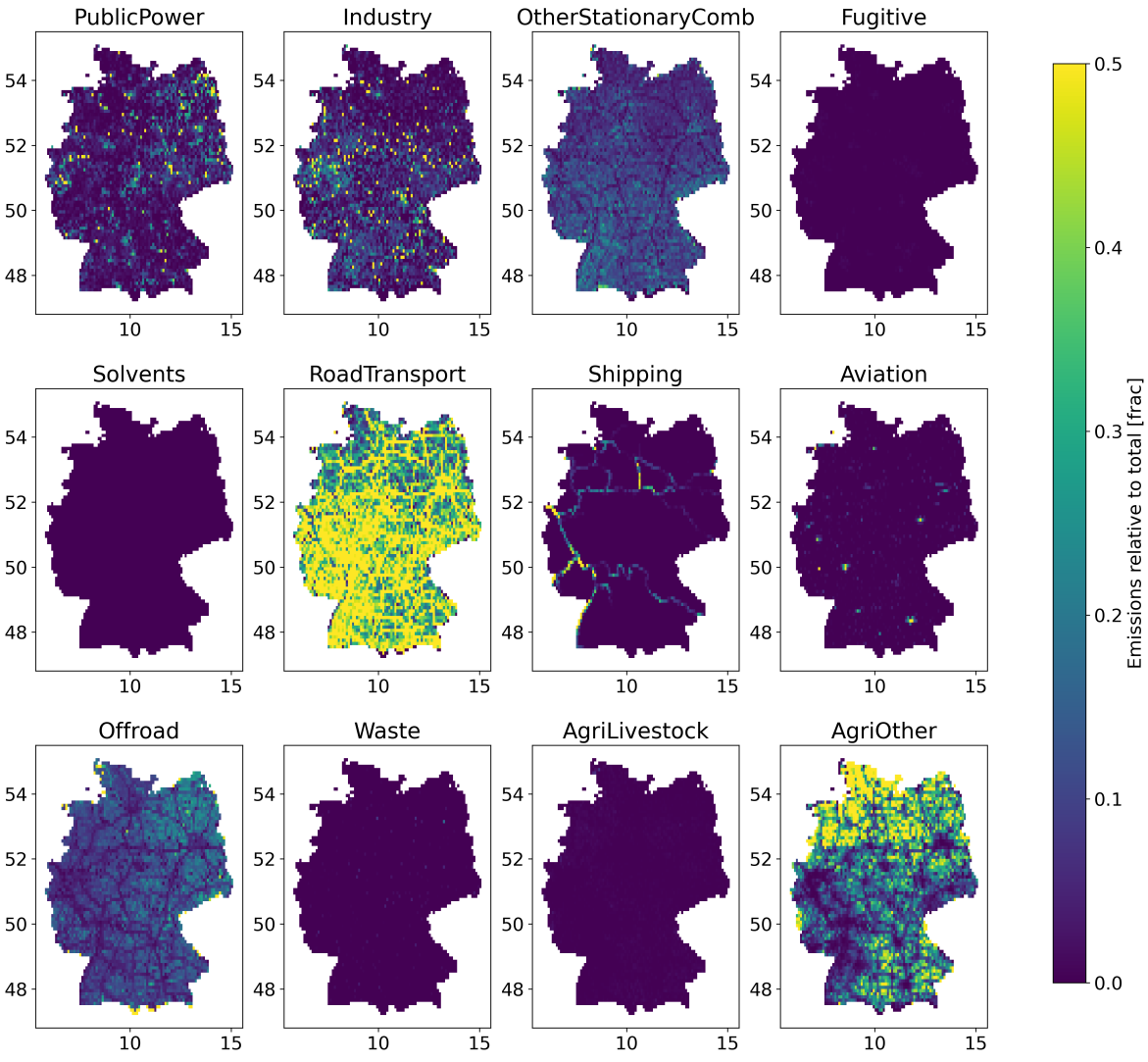

Figure A1. Fraction of emissions emitted by each emission sector for each grid cell within the German domain. Yellow indicates locations with emissions dominated (>50%) by an individual source sector. The displayed data is based on gridded GNFR inventory emissions of 2019.

https://doi.org/10.5194/gmd-2022-292
Preprint. Discussion started: 16 December 2022

Geoscientific Model Development
Discussions
Open Access
EGU

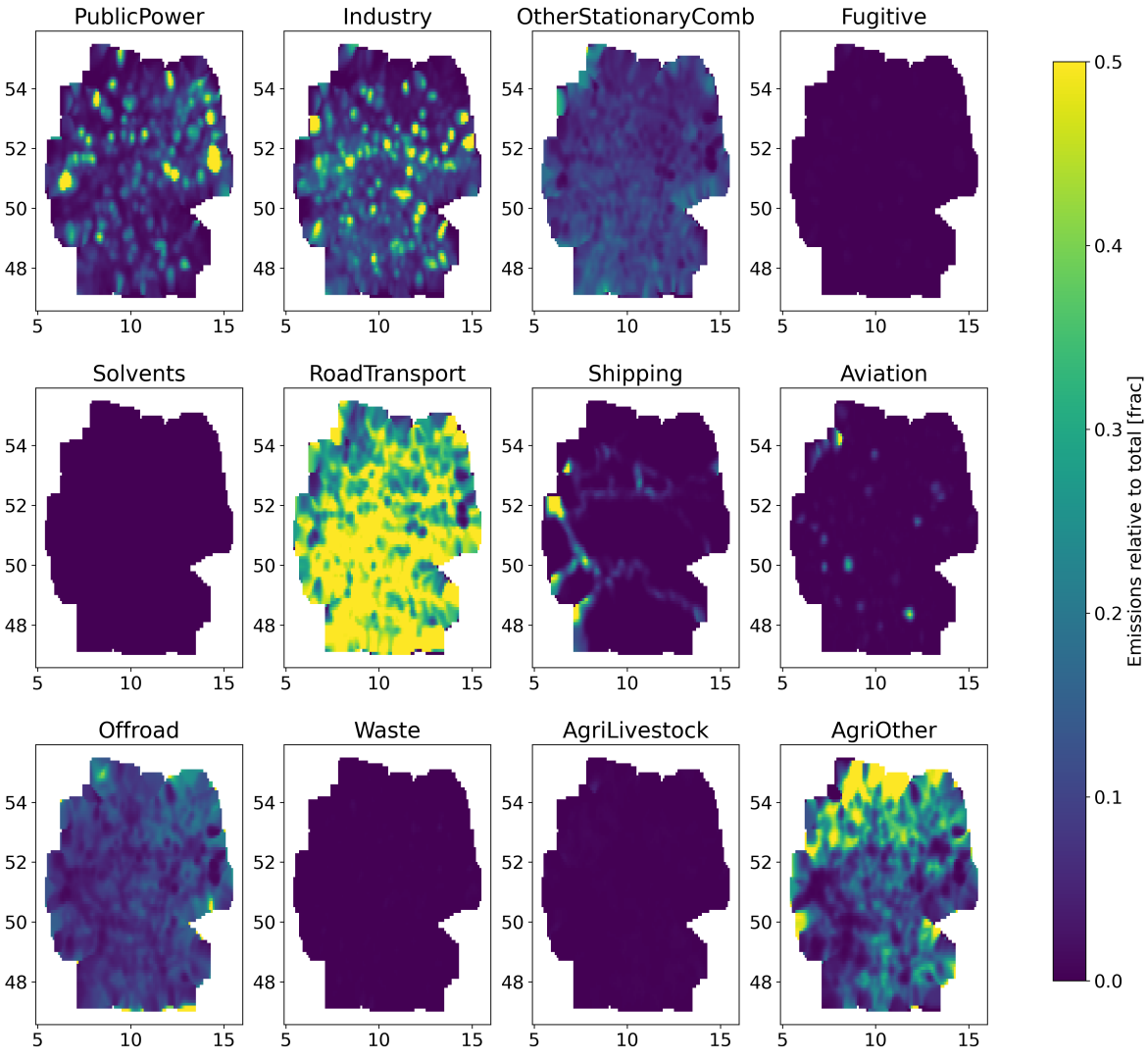

Figure A2. Fraction of emissions emitted by each emission sector for each grid cell within the German domain, smoothed with gaussian. The displayed data is based on gridded GNFR inventory emissions of 2019.

https://doi.org/10.5194/gmd-2022-292
Preprint. Discussion started: 16 December 2022

Geoscientific Model Development Discussions
Open Access
EGU

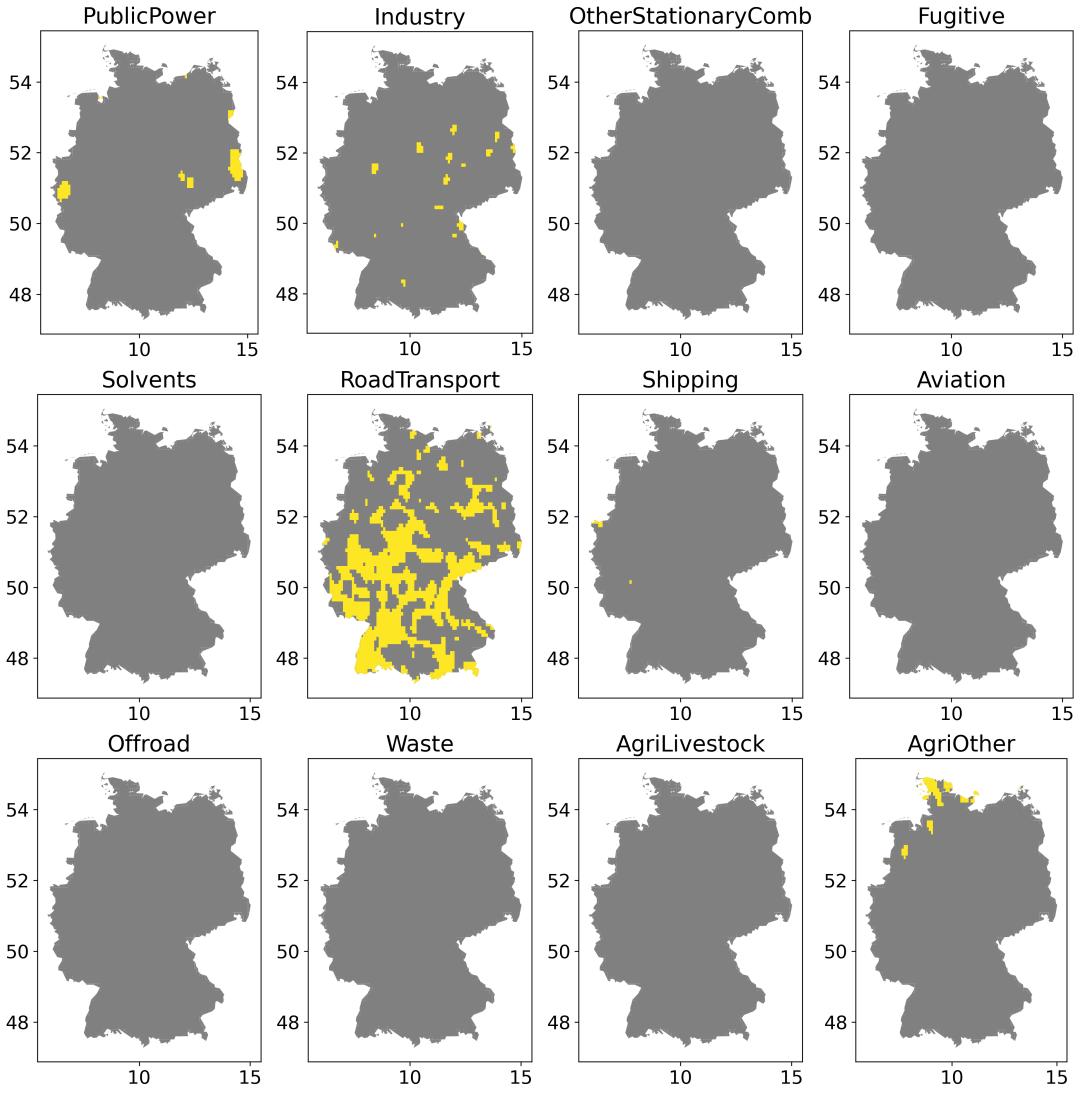

Figure A3. Emission source locations selected to produce sectoral trends. The produced masks are based on the results shown in Fig. A2, for all locations with an emission fraction above 50%. used to distinguish different source sectors in the emissions derived from satellite data.

https://doi.org/10.5194/gmd-2022-292
Preprint. Discussion started: 16 December 2022

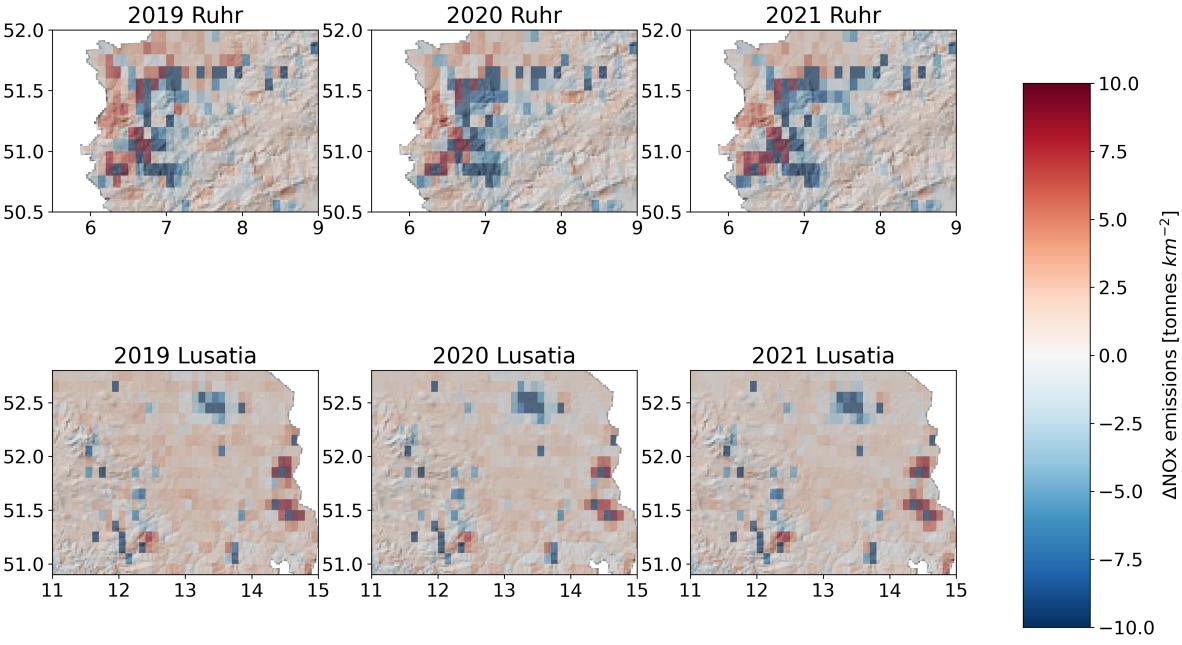

Figure A4. Difference between the satellite derived and inventory emissions (2019) for years 2019-2021 over two zoom regions. Upper row depicting the industrial "Ruhr" region, whilst the lower 3 panels show Lusatia at the eastern border of Germany.

https://doi.org/10.5194/gmd-2022-292
Preprint. Discussion started: 16 December 2022


Geoscientific Model Development Discussions

Author contributions. Enrico Dammers devised and implemented the methods presented in this paper and carried out the data analysis and writing of this publication together with Janot Tokaya, who made critical contributions to the data stream handling of the method (retrieval of the correct scenes, and CAMS meteorology data.) Renske Timmermans coordinated the scientific work from the TNO side and gave critical input to the scientific work with respect to the atmospheric chemistry of NO_x. Christian Mielke interpreted the spatial data of the algorithm runs and wrote the parts of the publication that deal with the emission inventory relevant topics. Kevin Hausmann designed and implemented the webtool and the level-0 emission estimation on the Code-DE Platform and provided the critical scientific environment for the success of this project. Debora Griffin and Chris McLinden helped devise the methods presented in this paper and gave critical input to the manuscript. Henk Eskes provided information on the satellite product. Finally, all authors discussed the results and reviewed the manuscript.

Competing interests. The authors declare that there are no competing interests present in carrying out the work presented in this publication.
The work has been financed by the Umweltbundesamt in the Leitplankenproject (FKZ: 3720515010).

Acknowledgements. We acknowledge the hard work done by KNMI, ESA, the team behind the PAL data portal, and the TROPOMI teams for making TROPOMI a success and providing easy access to the NO_2 data. ECMWF ERA5 data Hersbach et al. (2020) was downloaded from the Copernicus Climate Change Service (C3S) Climate Data Store. We thank Stefan Feigenspan for providing the 2019 GRETA data and for sharing his knowledge on emission gridding.

https://doi.org/10.5194/gmd-2022-292
Preprint. Discussion started: 16 December 2022

Geoscientific Model Development Discussions

References

Anderson, G. and Klugmann, D.: A European lightning density analysis using 5 years of ATDnet data, Natural Hazards and Earth System Sciences, 14, 815–829, https://doi.org/10.5194/nhess-14-815-2014, 2014.

Atkinson, R. W., Butland, B. K., Anderson, H. R., and Maynard, R. L.: Long-term concentrations of nitrogen dioxide and mortality: a meta-analysis of cohort studies, Epidemiology (Cambridge, Mass.), 29, 460, 2018.

Barré, J., Petetin, H., Colette, A., Guevara, M., Peuch, V.-H., Rouil, L., Engelen, R., Inness, A., Flemming, J., Pérez García-Pando, C., Bowdalo, D., Meleux, F., Geels, C., Christensen, J. H., Gauss, M., Benedictow, A., Tsyro, S., Friese, E., Struzewska, J., Kaminski, J. W., Douros, J., Timmermans, R., Robertson, L., Adani, M., Jorba, O., Joly, M., and Kouznetsov, R.: Estimating lockdown-induced European NO_2 changes using satellite and surface observations and air quality models, Atmospheric Chemistry and Physics, 21, 7373–7394, https://doi.org/10.5194/acp-21-7373-2021, 2021.

Beirle, S., Boersma, K. F., Platt, U., Lawrence, M. G., and Wagner, T.: Megacity emissions and lifetimes of nitrogen oxides probed from space, Science, 333, 1737–1739, 2011.

Beirle, S., Hörmann, C., Jöckel, P., Liu, S., Penning de Vries, M., Pozzer, A., Sihler, H., Valks, P., and Wagner, T.: The STRatospheric Estimation Algorithm from Mainz (STREAM): estimating stratospheric NO 2 from nadir-viewing satellites by weighted convolution, Atmospheric Measurement Techniques, 9, 2753–2779, 2016.

Beirle, S., Borger, C., Dörner, S., Eskes, H., Kumar, V., de Laat, A., and Wagner, T.: Catalog of NO_x emissions from point sources as derived from the divergence of the NO_2 flux for TROPOMI, Earth System Science Data, 13, 2995–3012, https://doi.org/10.5194/essd-13-2995-2021, 2021.

Belch, J. J., Fitton, C., Cox, B., and Chalmers, J. D.: Associations between ambient air pollutants and hospital admissions: more needs to be done, Environmental Science and Pollution Research, 28, 61 848–61 852, https://doi.org/10.1007/s11356-021-16544-0, 2021.

Bucsela, E. J., Pickering, K. E., Allen, D. J., Holzworth, R. H., and Krotkov, N. A.: Midlatitude Lightning NOx Production Efficiency Inferred From OMI and WWLLN Data, Journal of Geophysical Research: Atmospheres, 124, 13 475–13 497, https://doi.org/https://doi.org/10.1029/2019JD030561, 2019.

CLRTAP: National gridded data of emissions (CLRTAP), https://cdr.eionet.europa.eu/de/un/clrtap/gridded/envyizg6q/, 2021.

CLRTAP: LRTAP Convention - National emission inventories, https://cdr.eionet.europa.eu/de/un/clrtap/inventories/envygjjnq/index_html?, 2022.

Crippa, M., Guizzardi, D., Muntean, M., Schaaf, E., Lo Vullo, E., Solazzo, E., Monforti-Ferrario, F., Olivier, J., and Vignati, E.: EDGAR v5. 0 global air pollutant emissions, European Commission, Joint Research Centre (JRC)[Dataset] PID: http://data. europa. eu/89h/377801af-b094-4943-8fdc-f79a7c0c2d19, 2019.

Crutzen, P., FRITH, R., and HOUGHTON, J.: Absorption and emission by carbon-dioxide in mesosphere, Quarterly Journal of the Royal Meteorological Society, 96, 767, 1970.

Dammers, E., McLinden, C. A., Griffin, D., Shephard, M. W., Van Der Graaf, S., Lutsch, E., Schaap, M., Gainairu-Matz, Y., Fioletov, V., Van Damme, M., Whitburn, S., Clarisse, L., Cady-Pereira, K., Clerbaux, C., Coheur, P. F., and Erisman, J. W.: NH_3 emissions from large point sources derived from CrIS and IASI satellite observations, Atmospheric Chemistry and Physics, 19, 12 261–12 293, https://doi.org/10.5194/acp-19-12261-2019, 2019.

https://doi.org/10.5194/gmd-2022-292
Preprint. Discussion started: 16 December 2022

Geoscientific Model Development Discussions

Dammers, E., Shephard, M., Griffin, D., Chow, E., White, E., Hickman, J., Tokaya, J., Lutsch, E., Kharol, S., van der Graaf, S., Cady-Pereira, K., Bittman, S., Mclinden, C., Erisman, J., and Schaap, M.: County-level ammonia emissions monitored worldwide, Nature Geoscience, a, a, https://assets.researchsquare.com/files/rs-1752718/v1_covered.pdf?c=1656451952, 2022a.

Dammers, E., Tokaya, J., Timmermans, R., Schaap, M., and Coenen, P.: Final Report, Satellite-based Emission Verification, Pilot Study, linktoreport, 2022b.

de Foy, B., Wilkins, J. L., Lu, Z., Streets, D. G., and Duncan, B. N.: Model evaluation of methods for estimating surface emissions and chemical lifetimes from satellite data, Atmospheric Environment, 98, 66 – 77, https://doi.org/https://doi.org/10.1016/j.atmosenv.2014.08.051, 2014.

Ding, J., van der A, R. J., Eskes, H. J., Mijling, B., Stavrakou, T., van Geffen, J. H. G. M., and Veefkind, J. P.: NOx Emissions Reduction and Rebound in China Due to the COVID-19 Crisis, Geophysical Research Letters, 47, e2020GL089 912, https://doi.org/https://doi.org/10.1029/2020GL089912, e2020GL089912 2020GL089912, 2020.

Dore, C.: Technical Guidance for Emission Inventory Adjustments under the Amended Gothenburg Protocol: Inventory adjustments in context of ERCs, CEIP, a, a, https://doi.org/2514/06AL22/2310, 2022.

EEA: MEP/EEA air pollutant emission inventory guidebook 2019: Technical guidance to prepare national emission inventories', EEA Technical report, (12/2019), https://www.eea.europa.eu/publications/emep-eea-guidebook-2019, 2019.

EPH: Jänschwalde(Accessed on < 05-10-2022 >), https://www.eppowereurope.cz/en/companies/janschwalde/, 2022.

EU: Directive 2001/81/EC of the European Parliament and of the Council on national emission ceilings for certain atmospheric pollutants, http://eur-lex.europa.eu/LexUriServ/LexUriServ.do?uri=OJ:L:2001:309:0022:0030:EN:PDF, 2022.

Fioletov, V., McLinden, C., Krotkov, N., Moran, M., and Yang, K.: Estimation of SO2 emissions using OMI retrievals, Geophysical Research Letters, 38, 2011.

Fioletov, V., McLinden, C. A., Kharol, S. K., Krotkov, N. A., Li, C., Joiner, J., Moran, M. D., Vet, R., Visschedijk, A. J., van der Gon, D., et al.: Multi-source SO_2 emission retrievals and consistency of satellite and surface measurements with reported emissions, Atmospheric Chemistry and Physics, 17, 12 597–12 616, 2017.

Fioletov, V. E., McLinden, C. A., Krotkov, N., and Li, C.: Lifetimes and emissions of SO2 from point sources estimated from OMI, Geophysical Research Letters, 42, 1969–1976, https://doi.org/https://doi.org/10.1002/2015GL063148, 2015.

Goldberg, D. L., Lu, Z., Streets, D. G., de Foy, B., Griffin, D., McLinden, C. A., Lamsal, L. N., Krotkov, N. A., and Eskes, H.: Enhanced Capabilities of TROPOMI NO2: Estimating NO X from North American Cities and Power Plants, Environmental science & technology, 53, 12 594–12 601, 2019.

Goldberg, D. L., Anenberg, S. C., Griffin, D., McLinden, C. A., Lu, Z., and Streets, D. G.: Disentangling the impact of the COVID-19 lockdowns on urban NO2 from natural variability, Geophysical Research Letters, 47, e2020GL089 269, 2020.

Granier, C., Darras, H., Denier van der Gon, J., Doubalova, N., Elguindi, B., Galle, M., Gauss, M., Guevara, J., Jalkanen, J., and Kuenen, C.: The Copernicus Atmosphere Monitoring Service Global and Regional Emissions, Report April 2019 version (Research Report), ECMWF, Reading, UK, Reading, UK,[data set], 10, 2019.

Griffin, D., McLinden, C. A., Racine, J., Moran, M. D., Fioletov, V., Pavlovic, R., Mashayekhi, R., Zhao, X., and Eskes, H.: Assessing the impact of Corona-Virus-19 on nitrogen dioxide levels over Southern Ontario, Canada, Remote Sensing, 12, 4112, 2020.

Hersbach, H., Bell, B., Berrisford, P., Biavati, G., Horányi, A., Muñoz Sabater, J., Nicolas, J., Peubey, C., Radu, R., Rozum, I., Schepers, D., Simmons, A., Soci, C., Dee, D., and Thépaut, J.-N.: ERA5 hourly data on pressure levels from 1979 to present. Copernicus Climate Change Service (C3S) Climate Data Store (CDS). (Accessed on < 18-01-2022 >), https://doi.org/10.24381/cds.bd0915c6, 2018.

https://doi.org/10.5194/gmd-2022-292
Preprint. Discussion started: 16 December 2022

Hersbach, H., Bell, B., Berrisford, P., Hirahara, S., Horányi, A., Muñoz-Sabater, J., Nicolas, J., Peubey, C., Radu, R., Schepers, D., et al.: The ERA5 global reanalysis, 2020.

Jamali, S., Klingmyr, D., and Tagesson, T.: Global-Scale Patterns and Trends in Tropospheric NO2 Concentrations, 2005–2018, Remote Sensing, 12, 3526, 2020.

Kuenen, J., Dellaert, S., Visschedijk, A., Jalkanen, J.-P., Super, I., and Denier van der Gon, H.: CAMS-REG-v4: a state-of-the-art high-resolution European emission inventory for air quality modelling, Earth System Science Data, 14, 491–515, https://doi.org/10.5194/essd-14-491-2022, 2022.

Lorente, A., Boersma, K., Eskes, H., Veefkind, J., Van Geffen, J., De Zeeuw, M., Denier Van Der Gon, H., Beirle, S., and Krol, M.: Quantification of nitrogen oxides emissions from build-up of pollution over Paris with TROPOMI, Scientific reports, 9, 1–10, 2019.

Manders, A. M., Builtjes, P. J., Curier, L., van der Gon, D., Hugo, A., Hendriks, C., Jonkers, S., Kranenburg, R., Kuenen, J. J., Segers, A. J., et al.: Curriculum vitae of the LOTOS–EUROS (v2. 0) chemistry transport model, Geoscientific Model Development, 10, 4145–4173, https://doi.org/https://doi.org/10.5194/gmd-10-4145-2017, 2017.

McLinden, C., Griffin, D., Fioletov, V., Zhang, J., Dammers, E., Adams, C., Loria, M., Krotkov, N., and Lamsal, N.: Monitoring of total and off-road NOx emissions from Canadian oil sands surface mining using the Ozone Monitoring Instrument, To be submitted, Atmospheric Chemistry and Physics, can be shared, 2022.

McLinden, C. A., Fioletov, V., Shephard, M. W., Krotkov, N., Li, C., Martin, R. V., Moran, M. D., and Joiner, J.: Space-based detection of missing sulfur dioxide sources of global air pollution, Nature Geoscience, 9, 496–500, 2016.

McLinden, C. A., Adams, C. L., Fioletov, V., Griffin, D., Makar, P. A., Zhao, X., Kovachik, A., Dickson, N., Brown, C., Krotkov, N., et al.: Inconsistencies in sulfur dioxide emissions from the Canadian oil sands and potential implications, Environmental Research Letters, 16, 014 012, https://doi.org/https://doi.org/10.1088/1748-9326/abcbbb, 2020.

Mijling, B., Van Der A, R., Boersma, K., Van Roozendael, M., De Smedt, I., and Kelder, H.: Reductions of NO2 detected from space during the 2008 Beijing Olympic Games, Geophysical Research Letters, 36, 2009.

Miyazaki, K., Eskes, H., and Sudo, K.: Global NO x emission estimates derived from an assimilation of OMI tropospheric NO 2 columns, Atmospheric Chemistry and Physics, 12, 2263–2288, 2012.

Nations., U.: 1979 Convention on Long-Range Transboundary Air Pollution, https://treaties.un.org/Pages/ViewDetails.aspx?src=IND&mtdsg_no=XXVII-1&chapter=27&clang=_en, 1979.

Organization, W. H. et al.: WHO global air quality guidelines: particulate matter (PM2. 5 and PM10), ozone, nitrogen dioxide, sulfur dioxide and carbon monoxide, World Health Organization, https://www.who.int/publications/i/item/9789240034228, 2021.

Paige, C. C. and Saunders, M. A.: LSQR: An Algorithm for Sparse Linear Equations and Sparse Least Squares, ACM Trans. Math. Software, pp. 43–71, 1982.

Pommier, M., McLinden, C. A., and Deeter, M.: Relative changes in CO emissions over megacities based on observations from space, Geophysical research letters, 40, 3766–3771, https://doi.org/https://doi.org/10.1002/grl.50704, 2013.

Schneider, C., Pelzer, M., Toenges-Schuller, N., Nacken, M., and Niederau, A.: ArcGIS basierte Lösung zur detaillierten, deutschlandweiten Verteilung (Gridding) nationaler Emissionsjahreswerte auf Basis des Inventars zur Emissionsberichterstattung: Forschungskennzahl 3712 63 240 2, Texte, 71, 5, 2016.

Simpson, D.: Copernicus Atmosphere Monitoring Service soil global NOx emissions (CAMS-GLOB-SOIL v2.2), https://doi.org/https://doi.org/10.24380/kz2r-fe18, 2022.

https://doi.org/10.5194/gmd-2022-292
Preprint. Discussion started: 16 December 2022

Simpson, D. and Darras, S.: Global soil NO emissions for Atmospheric Chemical Transport Modelling: CAMS-GLOB-SOIL v2.2, Earth System Science Data Discussions, 2021, 1–35, https://doi.org/10.5194/essd-2021-221, 2021.

Simpson, D., Winiwarter, W., Börjesson, G., Cinderby, S., Ferreiro, A., Guenther, A., Hewitt, C. N., Janson, R., Khalil, M. A. K., Owen, S., et al.: Inventorying emissions from nature in Europe, Journal of Geophysical Research: Atmospheres, 104, 8113–8152, https://doi.org/https://doi.org/10.1029/98JD02747, 1999.

van der Walt, S., Schönberger, J. L., Nunez-Iglesias, J., Boulogne, F., Warner, J. D., Yager, N., Gouillart, E., Yu, T., and the scikit-image contributors: scikit-image: image processing in Python, PeerJ, 2, e453, https://doi.org/10.7717/peerj.453, 2014.

van Geffen, J., Eskes, H., Compernolle, S., Pinardi, G., Verhoelst, T., Lambert, J.-C., Sneep, M., ter Linden, M., Ludewig, A., Boersma, K. F., and Veefkind, J. P.: Sentinel-5P TROPOMI NO_2 retrieval: impact of version v2.2 improvements and comparisons with OMI and ground-based data, Atmospheric Measurement Techniques, 15, 2037–2060, https://doi.org/10.5194/amt-15-2037-2022, 2022.

Vattenfall: Vattenfall to phase-out 1,000 MW lignite capacity (Accessed on < 05-10-2022 >), https://group.vattenfall.com/press-and-media/pressreleases/2015/vattenfall-to-phase-out-1000-mw-lignite-capacity, 2015.

Veefkind, J. P., Aben, I., McMullan, K., Förster, H., de Vries, J., Otter, G., Claas, J., Eskes, H. J., de Haan, J. F., Kleipool, Q., van Weele, M., Hasekamp, O., Hoogeveen, R., Landgraf, J., Snel, R., Tol, P., Ingmann, P., Voors, R., Kruizinga, B., Vink, R., Visser, H., and Levelt, P. F.: TROPOMI on the ESA Sentinel-5 Precursor: A GMES mission for global observations of the atmospheric composition for climate, air quality and ozone layer applications, rse, 120, 70–83, https://doi.org/10.1016/j.rse.2011.09.027, 2012.

Verhoelst, T., Compernolle, S., Pinardi, G., Lambert, J.-C., Eskes, H. J., Eichmann, K.-U., Fjæraa, A. M., Granville, J., Niemeijer, S., Cede, A., Tiefengraber, M., Hendrick, F., Pazmiño, A., Bais, A., Bazureau, A., Boersma, K. F., Bognar, K., Dehn, A., Donner, S., Elokhov, A., Gebetsberger, M., Goutail, F., Grutter de la Mora, M., Gruzdev, A., Gratsea, M., Hansen, G. H., Irie, H., Jepsen, N., Kanaya, Y., Karagkiozidis, D., Kivi, R., Kreher, K., Levelt, P. F., Liu, C., Müller, M., Navarro Comas, M., Piters, A. J. M., Pommereau, J.-P., Portafaix, T., Prados-Roman, C., Puentedura, O., Querel, R., Remmers, J., Richter, A., Rimmer, J., Rivera Cárdenas, C., Saavedra de Miguel, L., Sinyakov, V. P., Stremme, W., Strong, K., Van Roozendael, M., Veefkind, J. P., Wagner, T., Wittrock, F., Yela González, M., and Zehner, C.: Ground-based validation of the Copernicus Sentinel-5P TROPOMI NO_2 measurements with the NDACC ZSL-DOAS, MAX-DOAS and Pandonia global networks, Atmospheric Measurement Techniques, 14, 481–510, https://doi.org/10.5194/amt-14-481-2021, 2021.

Virtanen, P., Gommers, R., Oliphant, T. E., Haberland, M., Reddy, T., Cournapeau, D., Burovski, E., Peterson, P., Weckesser, W., Bright, J., van der Walt, S. J., Brett, M., Wilson, J., Millman, K. J., Mayorov, N., Nelson, A. R. J., Jones, E., Kern, R., Larson, E., Carey, C. J., Polat, İ., Feng, Y., Moore, E. W., VanderPlas, J., Laxalde, D., Perktold, J., Cimrman, R., Henriksen, I., Quintero, E. A., Harris, C. R., Archibald, A. M., Ribeiro, A. H., Pedregosa, F., van Mulbregt, P., and SciPy 1.0 Contributors: SciPy 1.0: Fundamental Algorithms for Scientific Computing in Python, Nature Methods, 17, 261–272, https://doi.org/10.1038/s41592-019-0686-2, 2020.

Wang, Z., Bovik, A. C., Sheikh, H. R., and Simoncelli, E. P.: Image quality assessment: from error visibility to structural similarity, IEEE transactions on image processing, 13, 600–612, 2004.

Yienger, J. J. and Levy II, H.: Empirical model of global soil-biogenic $NO\chi$ emissions, Journal of Geophysical Research: Atmospheres, 100, 11 447–11 464, https://doi.org/https://doi.org/10.1029/95JD00370, 1995.

Zhao, X., Fioletov, V., Alwarda, R., Su, Y., Griffin, D., Weaver, D., Strong, K., Cede, A., Hanisco, T., Tiefengraber, M., McLinden, C., Eskes, H., Davies, J., Ogyu, A., Sit, R., Abboud, I., and Lee, S. C.: Tropospheric and Surface Nitrogen Dioxide Changes in the Greater Toronto Area during the First Two Years of the COVID-19 Pandemic, Remote Sensing, 14, https://doi.org/10.3390/rs14071625, 2022.